An Efficient Feature Selection and Explainable Classification Method for EEG-based Epileptic Seizure Detection

Ijaz Ahmad^{a,b,c}, Chen Yao^d, Lin Li^e, Yan Chen^e, Zhenzhen Liu^e, Inam Ullah^f, Mohammad Shabaz^g, Xin Wang^{a,b,c}, Kaiyang Huang^h, Guanglin Li^{a,c}, Guoru Zhao^{a,c,*}, Oluwarotimi Williams Samuel^{i,j,*}, Shixiong Chen^{a,c,*}

Abstract

Epilepsy is a prevalent neurological disorder that poses life-threatening emergencies. Early electroencephalogram (EEG) seizure detection can mitigate the risks and aid in the treatment of patients with epilepsy. Electroencephalogram (EEG) based automatic epileptic seizure (ES) detection has significant applications in epilepsy treatment and medical diagnosis. Therefore, this paper presents an innovative framework

CAS Key Laboratory of Human-Machine Intelligence Synergy Systems, Shenzhen Institutes of Advanced Technology, Chinese Academy of Sciences, Shenzhen 518055, Guangdong, China.
 b Shenzhen College of Advanced Technology, University of Chinese Academy of Sciences, Shenzhen 518055, Guangdong, China.

^c Guangdong-Hong Kong-Macao Joint Laboratory of Human-Machine Intelligence-Synergy Systems, Shenzhen 518055, Guangdong, China.

Department of Neurosurgery, The National Key Clinic Specialty, Shenzhen Key Laboratory of Neurosurgery, the First Affiliated Hospital of Shenzhen University, Shenzhen Second People's Hospital,3002 # Sungang Road, Futian District, Shenzhen 518055, Guangdong, China.

^e The National Key Clinic Specialty, Shenzhen Key Laboratory of Neurosurgery, the First Affiliated Hospital of Shenzhen University, Shenzhen Second People's Hospital, 3002# Sungang Road, Futian District, Shenzhen 518035, China.

f Department of Computer Engineering, Gachon University, Seongnam 13120, Republic of Korea.
g The Model Institute of Engineering and Technology, Jammu, J& K, India.

^h The Medical Information Engineering, Guangzhou University of Chinese Medicine, Guangzhou 510405, Guangdong, China.

ⁱ School of Computing, University of Derby, Derby, DE22 3AW, United Kingdom.

^j Data Science Research Centre, University of Derby, Derby, DE22 3AW, United Kingdom.

^{*}Corresponding authors.

 $Email\ address:$ sx.chen@siat.ac.cn (Shixiong Chen), gr.zhao@siat.ac.cn (Guoru Zhao), o.samuel@derby.ac.uk (Oluwarotimi Williams Samuel) ()

for automatic ES detection using coefficient and distance correlation feature selection algorithms, a Bagged Tree-based classifier, and Explainable artificial intelligence (XAI). Initially, the Butterworth filter is employed to eliminate various artifacts, and the discrete wavelet transform (DWT) is used to decompose the EEG signals and extract 24 eigenvalue features of the statistical time domain (STD) as linear and Fractal dimension-based non-linear (FD-NL). The optimal features are then identified through correlation coefficients with P-value and distance correlation analysis. These features are subsequently utilized by the proposed Bagged Tree-based classifier. The model provides superior performance in mitigating overfitting issues and improves the average accuracy by 4% using (CD, E), (AB, CD, E), and (A, B) combination sets as compared to other machine learning (ML) models using well-known Bonn and UCI-EEG benchmark datasets. Finally, SHapley additive exPlanation (SHAP) was used as an Explainable AI (XAI) to interpret and explain the decisionmaking process of the proposed model. The results highlight the framework's capability to accurately classify ES, thereby improving the diagnosis process in patients with brain dysfunctions.

Keywords: Electroencephalogram, machine learning, coefficient correlation, distance correlation, biomedical signals, explainable artificial intelligence.

1. Introduction

Epilepsy is a noncontagious brain disorder that develops from irregular electrical brain activity [1, 2]. A delay in the diagnosis process can create severe mental health problems or even lead to death [3]. Globally, over sixty million people have been affected by the epilepsy disease reported by the World Health Organization (WHO) [4]. In order to mitigate the progression of the disease, the early diagnosis and detection of epileptic seizures (ES) are crucial. Recently, various diagnostic

approaches have captured the attention of specialized medical professionals for the diagnosis of epilepsy [5]. Moreover, neurologists recommended electroencephalography (EEG) to monitor the brain electrical activity of the seizure [6]. Conventional epilepsy diagnosis in clinical settings involves specialists visually inspecting during EEG recordings, which is laborious and intensive work. [7, 8]. Therefore, Machine Learning (ML) models have been introduced for efficient analysis by classifying EEG signals [8]. Moreover, existing automated EEG ES detection approaches are often less used in real-time clinical applications because of their low sensitivity and specificity in clinical epilepsy management. Several challenges exist in the automation of EEG ES detection. Primarily, the extraction of highly representative features is challenging because of the nonlinear and non-stationary nature of EEG signals [8]. Secondly, the optimal features of the EEG are very important. It poses efficient features to identify the differentiation between pre-ictal and seizure states while also learning the patterns' complexity and variability across seizure types. The third challenge pertains to minimizing the miss classification rate, arising from the similarities in oscillatory and fractal characteristics across seizure and non-seizure EEG signals [7]. The fourth challenge includes the interoperability and explainability of the ML model, which are essential for informed clinical decisions and enhancing patient safety. To address the above informative challenges, this study presents a novel framework for the automatic detection of EEG ES utilizing biomedical EEG signals. The framework consists of a feature extraction method that exploits distinctive FD-nonlinear (FD-NL) and statistical time domain (STD) features extracted from decomposed EEG signal sub-bands, capturing the EEG signals' nonlinear and time-domain information. The proposed study also employs correlation coefficients (CC) for linear feature selection and distance correlation (DC) for non-linear feature selection in EEG ES detection. Additionally, the proposed study employs a Bagged

Tree-based classifier to enhance the accuracy of ES classification. Moreover, the proposed study also uses explainable AI (XAI) to explain the decision-making processes behind the model's detection. XAI facilitates a transparent and understandable explanation of ML model or algorithm decisions [9, 10], which is especially important in ES detection by providing clinicians insights into the decision-making process. The proposed framework, with the integration of XAI, aims to enhance the diagnostic decision-making process in clinical practice. The proposed study is summarized as follows:

• The EEG signals are split and decomposed by using the Discrete Wavelet Transform (DWT). From the different decomposition levels, the statistical time domain (STD) and Fractal dimension-based non-linear (FD-NL) features are extracted.

45

50

55

- Applied Correlation Coefficients (CC) and Distance Correlation (DC) feature selection methods to select the optimal features of STD and FD-NL through correlation with p-value analysis and distance correlation.
- The implementation of the bagged Tree-based classifier is designed to mitigate overfitting by introducing randomness and diversity into the ensemble, thereby enhancing its capability to accurately classify epileptic seizures.
 - The development of an explainable artificial intelligence (XAI) framework utilizing the SHAP (SHapley Additive exPlanations) model has an explanation behind the reasoning of the proposed model predictions. The visual explanations generated by SHAP facilitate a deeper understanding of the interpretive processes underlying the decisions of the most effective classifiers, as well as identifying the critical features for the detection of epileptic seizures (ES).

The proposed EEG ES detection framework enhances accuracy, mitigates overfitting, and enables optimal feature selection. Tested on the Bonn and UCI-EEG datasets, its versatility and comprehensive approach show promise for streamlining diagnostics and improving patient outcomes.

The organization of the paper is as follows: Section 1 and 2 present the introduction and related works, respectively. Sections 3 show the automatic EEG ES detection framework. Experimental results and discussion are discussed in sections 4 and 5, respectively. Finally, the conclusion of the paper is in section 6.

2. Related Work

This section describes the prior research that used various decomposition methods, linear and non-linear features, optimal feature selection methods, and ML models for efficiently detecting epileptic seizures (ES) using electroencephalogram (EEG) data.

2.1. Wavelet-based statistical and fractal dimension (FD) feature extraction with machine learning models

The extraction of important and essential features is important, especially from different wavelet decomposition levels, in EEG epileptic seizure detection. Various studies have applied wavelet-based features for accurate classification of pre-ictal, inter-ictal, and ictal states in EEG-based ES detection [11, 12, 13, 14, 15].

Recently, Al-Salman et al. [11] applied discrete wavelet transform (DWT) to decompose brain EEG signals into subbands, further processing to extract diverse wavelet-based features. A Grey Wolf Optimizer (GWO) based deep recurrent neural network (DRNN) was employed to differentiate between seizure and non-seizure signals, achieving 93.4 % accuracy in automatic EEG ES detection. Harender et al.

[16] employed DWT for EEG signal decomposition and extracted statistical features like standard deviation (std) and mean absolute value (MAV), achieving over 90% accuracy using K-Nearest Neighbors (KNN) classifiers. Sharmila et al. [17] applied DWT for EEG signal decomposition and extracted statistical features (std, average power (AVP), and MAV) with KNN and Naive Bayes (NB) classifiers, obtaining 98% accuracy with KNN. Moreover, R. Uthayakumar et al. [18] introduced six waveletbased statistical time domain (STD) features, such as variance and std, with several ML models, where the Decision Tree (DT) model achieved 97% accuracy. In the last two decades, Fractal Dimension (FD) feature extraction techniques have received much attention, exhibiting satisfactory performance with various feature selection methods and ML [18, 19, 20]. A study [18] introduced an automated system for ES detection using FD theory and the Support Vector Machine (SVM) model, achieving up to 90% accuracy. T. M. E. Nijsen et al. [19] implemented various wavelet-based features, such as Higuchi's Fractal Dimension (HFD), Hurst Exponent (HE), and Shannon entropy, in combination with RF and SVM models. Hussain et al. [21] utilized DWT in the preprocessing stage, extracting HFD and Katz Fractal Dimension (KFD) features from DWT subbands and employing SVM for classification. Further, in [22, 23], Cross-Information Potential (CIP) and Tunable-Q Wavelet Transform (TQWT) were examined for EEG signal preprocessing, and the Random Forest (RF) model was used for classification, achieving satisfactory results. A. Nishad et al. [23] employed DWT for decomposition and extracted non-linear features, such as entropy and fractal dimensions and applied a Support Vector Machine (SVM) classifier, where fractal dimensions achieved above 96% overall accuracy. Upadhyay et al. [24] applied the Max Energy to Shannon Entropy ratio to select appropriate EEG channels from each frequency band, calculating three distinct non-linear features and using three machine learning techniques, where Least Square-Support Vector Machine (LS-SVM) showed satisfactory performance. The summary of the various literature shows the importance of STD linear and FD-non linear features with effective ML models in EEG epileptic seizure detection [25, 26, 27].

2.2. Correlation-based feature selection methods with the machine model

Feature selection is an important process that minimizes the number of features utilized by the ML model in EEG epileptic seizure detection. The reduction not only simplifies the model's complexity but also facilitates easier interpretation and decreases training time, often leading to enhanced system performance. Correlation, often measured as the relationship between two or more variables, has been widely applied in various fields over the past few decades due to its capability to measure both linear and nonlinear associations between features [13]. Aliyu et al. [14] introduced the Pearson correlation coefficient (PCC) in the feature selection process, aiming to identify the most pertinent subset of features from the original set. Upon selecting the optimal features via PCC, the model achieved an accuracy of 93.1%. Recently, N.Ji et al. [28] introduced an improved correlation-based feature selection method. The proposed methods select the optimal features from the time, frequency, and entropy features of wavelet decomposition, after which the random forest model performs classification, achieving 96% accuracy.

2.3. Motivation

130

After summarizing the above literature, we are motivated to present a correlation coefficient and distance correlation-based feature selection algorithms, a Bagged Tree-based classifier model with explainable AI (XAI).

For the feature selections, we employ p-value analysis to select dominant features, which eliminates the high-correlation features. A Bagged Tree-based classifier is then efficiently applied to differentiate EEG brain signals of seizure and non-seizure EEG states, while the explainable AI interprets and explains the decision-making process of the proposed algorithm automatically without any complex calculation or manual explanation.

The next section provides detailed information about the proposed framework for EEG ES detection.

3. Materials and Methods

This section presents a novel framework for automatic EEG-based epileptic seizure detection. The framework includes a detailed pipeline for EEG ES detection that presents the EEG data sets, preprocessing, feature extraction, feature selection, and explainable classification steps. Figure 1 provides the proposed framework for EEG ES detection.

3.1. EEG data collection

145

150

Initially, the collected EEG datasets from the UCI and Bonn EEG benchmark datasets are investigated. The Bonn EEG dataset includes non-seizure, transition, and seizure signals [15], while the UCI-EEG dataset consists of non-seizure and seizure signals [16].

3.1.1. Bonn EEG dataset

The Bonn EEG dataset was collected from the five patients [15]. The Bonn EEG dataset is categorized into five sets, labeled (A) through (E), each containing 100 single-channel EEG samples collected over 23.6 seconds [18]. The sampling rate of the Bonn EEG data set is 173.61 Hz. Sets A to E involve various states. Specifically, sets (A) and (B) represent different normal EEG signals, with (A) and (B) showing

Table 1: Notation Table

Notation	Description
$mean_1$	Mean feature from decomposition level D3
$mean_2$	Mean feature from decomposition level D4
$mean_3$	Mean feature from decomposition level D5
$mean_4$	Mean feature from decomposition level A5
std _1	standard deviation feature from decomposition
	level D3
std_2	Standard deviation feature from decomposition
	level D4
std_3	Standard deviation feature from decomposition
	level D5
std_4	Standard deviation feature from decomposition
	level A5
HFD_1	Nonlinear feature from decomposition level D3
ENT_2	Nonlinear feature from decomposition level D4
PFD_3	Nonlinear feature from decomposition level D5
HFD_4	Standard deviation feature from decomposition
	level A5

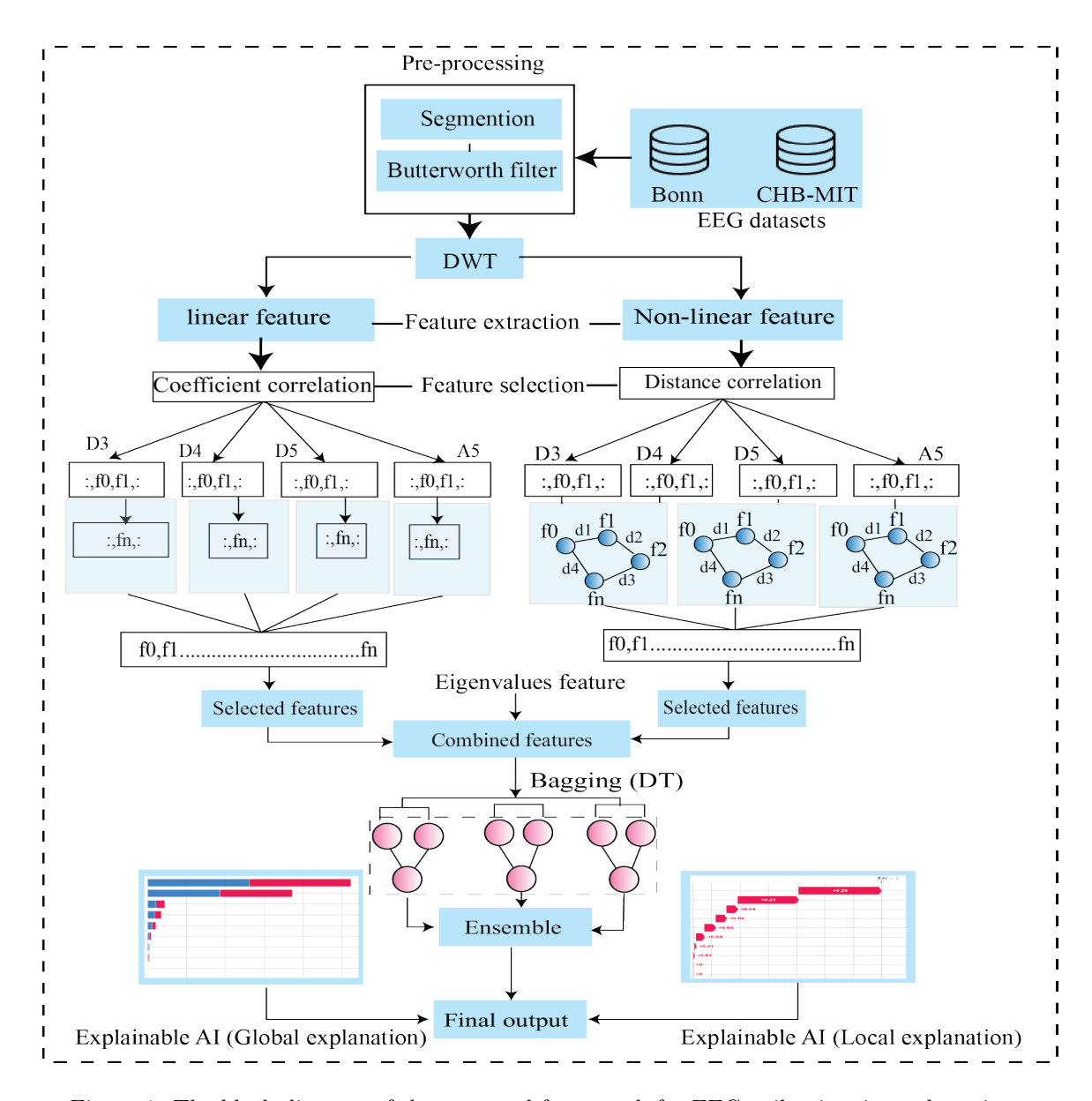


Figure 1: The block diagram of the proposed framework for EEG epileptic seizure detection.

EEG states where the subjects' eyes were open and closed, respectively. Sets C and D encompass transitional states between normal and seizure, while set (E) contains EEG readings from five EEG epileptic individuals during seizures. Sets (A) and (B)

were obtained non-invasively using the '10-20' international system, and sets (C) and (D) employed invasive recording methods [18]. Further details of each set within the Bonn EEG dataset are shown in Table 2, and Fig. 2 illustrates EEG epileptic seizures in non-seizure, transition, and seizure states.

Table 2: The detailed description of the Bonn EEG dataset.

Classification set	Stages	Segment	Number of files
		length	
(A)	Patient eyes opened	(69,1008)	100
(B)	Patient eyes closed	(69,1008)	100
(C)	Inter-ictal	(69,1008)	100
(D)	Inter-ictal	(69,1008)	100
(E)	Ictal	(69,1008)	100

3.1.2. UCI- EEG dataset

170

The UCI-EEG dataset was collected from 5 subjects, each with 4097 data points recorded over 23.5 seconds [27]. Each data point was segmented into 23 chunks, representing 1 second of EEG data. After segmentation, chunks were shuffled. The states of the subjects fluctuated between having their eyes open and having them closed. The target variable 'y', located in column 179, is a binary class y (0,1) used for analysis. It denotes the ictal and pre-ictal states, as detailed in Table 3. In addition, various EEG states of the UCI-EEG dataset are shown in Fig. 3.

In addition, various EEG states of the UCI-EEG dataset are shown in Figure 3.

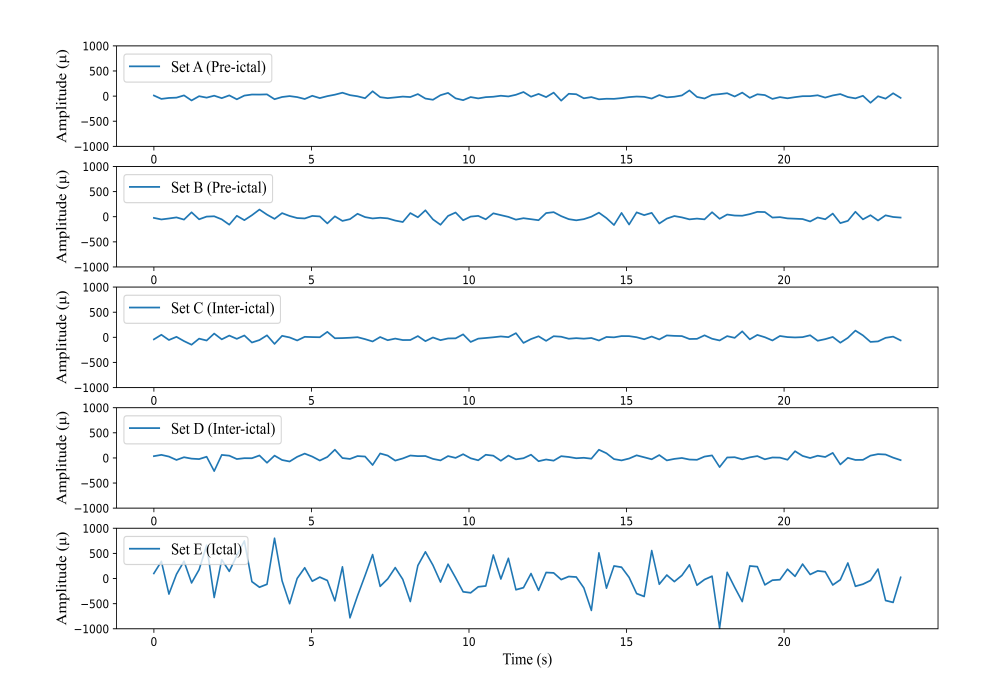


Figure 2: Various types of EEG signals in the Bonn dataset (Interictal, Pre-ictal, and Ictal).

Table 3: Full description of the UCI-EEG dataset.

Classification set	Stages	Segment	Number of
		length	files
(A)	Ictal	(86,1338)	100
(B)	Tumour region	(86,1338)	100
(C)	Healthy region	(86,1338)	100
(D)	Healthy region	(86,1338)	100

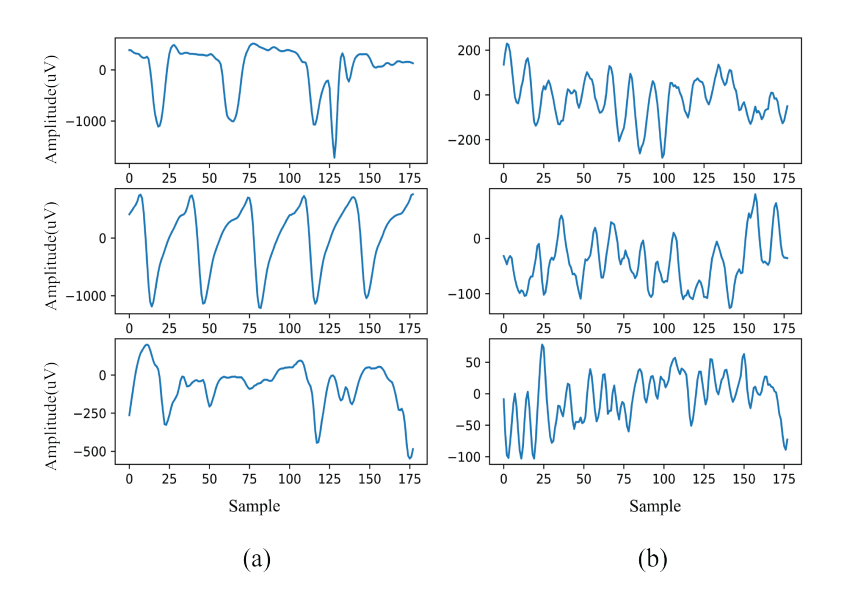


Figure 3: EEG signals in the UCI-EEG dataset. (a) Ictal, (b) Pre-ictal .

3.2. Pre-processing

In this section, the collected EEG signals pass through a filtering process to eliminate noise and artifacts that could originate from electromyography (EMG), eye blinking, or limb movements during recordings [23, 26]. A Butterworth filter is applied to maintain EEG signals within the desired frequency ranges, excluding noise. The Butterworth filter can be mathematically expressed as:

$$X(t)_{k-l} = BWF(y(t), k, l), k = 0, l = 100$$
(1)

where k and l denote the frequency range, y(t) represents the signals being filtered, and $cutof_freq = 0.1$, $filt_ororder = 3$, and $Nyquist_freq = 0.5$. To equalize sample quantities in the UCI-EEG dataset, the Synthetic Minority Oversampling Technique (SMOTE) is applied.

3.3. Signal Splitting

In the preprocessing subsection, we define the optimal segment size dividing the EEG signal time series into smaller epochs. For the Bonn EEG dataset, we increase the segment size using the optimal values of epoch = 0.4, segments = 69, and epoch_step = 0.024 as shown in Table 2. For the UCI dataset, the optimal segment size is epoch = 0.5, segments = 86, and epoch_step = 0.023 as shown in Table 3.

Algorithm 1 EEG Signals Splitting

- 1: Load the EEG signal t time series data; k = 0
- 2: Proper size of window w_{size}
- 3: while k > 0 do
- 4: select window size w_{size} and overlap w_{over}
- 5: Calculate the performance of w_{size} and w_{over}
- 6: k++
- 7: Calculated the performance of the feature vector
- 8: end while

3.4. EEG Signals decomposition and feature extraction

This subsection emphasizes the decomposition of the EEG signals and critical feature extraction from the EEG signals, enabling distinctive and analytical exploration of EEG data. The proposed feature extraction methods are explained in Algorithm 2 and have two primary steps: (1) EEG signal decomposition and (2) feature extraction. The non-stationary nature of EEG time-series signals, which contain high-frequency data and other important information, as well as large frequency oscillations, employing solely the fast Fourier transform (FFT) for signal analysis, proves insufficient due to its limitation to extracting merely the frequency

information of time-series signals [17]. The wavelet transform method of multiresolution analysis disassembles signals into various frequency bands and represents a time function using fundamental units called wavelets. One significant advantage of wavelet transforms is their ability to adapt the window size, enabling them to narrow for low frequencies and widen for high frequencies. This adaptability results in superior time-frequency resolution across different frequency bands. EEG signals, which contain a rich set of data points, can be effectively compressed into a reduced set of features through spectral analysis and the extraction of high-frequency data. The continuous wavelet transform (CWT) and discrete wavelet transform (DWT) are mathematically represented as follows:

$$CWT_{(c,d)} = \int_{-\infty}^{\infty} y_t \psi_{c,d} * y(y) dy$$
 (2)

where y_t presents the investigated EEG signal, and c represents the compression coefficient with dilation, translation, and scaling relevant to the time axis. The asterisk superscript denotes complex conjugation. Additionally, $\psi_{c,d}$ is computed as the wavelet over time and scale:

$$\psi_{c,d}(t) = \frac{1}{\sqrt{|c|}} \psi(\frac{t-d}{c}) \tag{3}$$

Where $\psi_{c,d}(t)$ shows the wavelet, and CWT translation and scaling parameters can be changed continuously. However, determining wavelet coefficients for every possible scale can be computationally intensive and produce considerable data. The wavelet transform is an extension of the conventional Fourier transform.

Initially, the input signals x[n] are segmented into low-pass g[n] and high-pass h[n] filters. The output from these filters is represented by coefficient D1 and approximation A1, respectively. Symbols D_n and A_n denote the frequencies of the input EEG signals. The decomposition process is iteratively performed to acquire subsequent

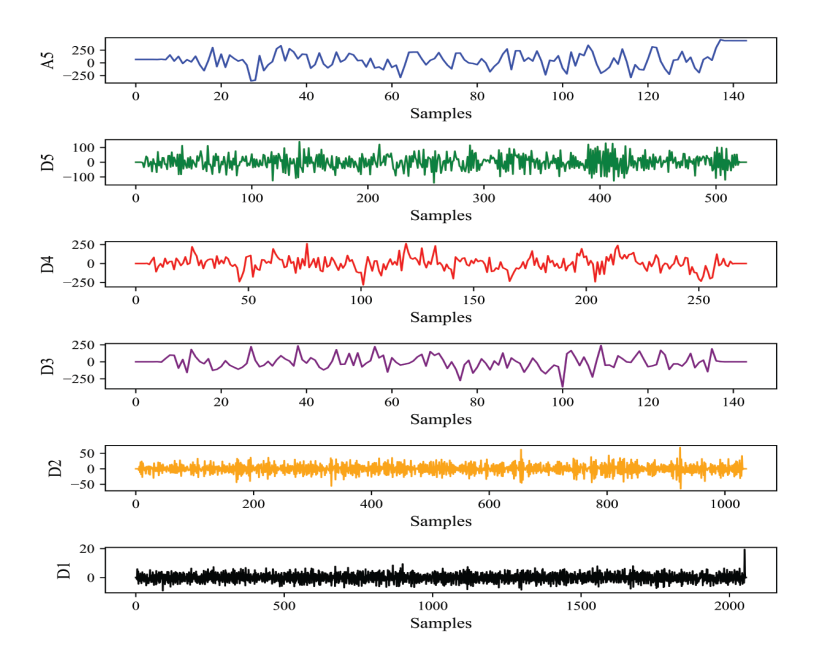


Figure 4: The decomposition level of Bonn data using DWT.

coefficient levels, with a five-level decomposition being executed in this study. Each step of decomposition enhances frequency resolution while down-sampling diminishes time resolution, as illustrated in Figure 4.

The same procedure is applied to the UCI-EEG dataset using the Daubechies 4 (db4) wavelet. Each decomposition level captures the important frequency components essential for seizure detection in EEG signals as shown in Table .4.

For seizure detection, the frequency range is typically from 2 to 30 Hz. As a result, the coefficients D1 and D2 are removed from processing due to their high-frequency range. Thus, the approximation coefficients (D3; D4; D5; A5) of each channel are considered. In this study, each subband encompasses 24 FD-based nonlinear and statistical features from both the Bonn and UCI-EEG datasets.

Table 4: Decomposition levels of the EEG signals of various frequency (Hz).

Sub-band	Frequency (Hz)	Decomposition level
Detail D5	[3-6]	5
Detail D4	[6-12]	4
Detail D3	[12-15]	3
Detail D2	[25-50]	2
Detail D1	[50-100]	1

3.5. Feature extraction methods

230

This subsection discusses the feature extraction process from each subband, including different FD-based non-linear (FD-NL) and statistical time domain (STD) features [21]. These features are important for describing the characteristics of the EEG signals and enabling differentiation between various EEG states. FD-nonlinear features, extracted from the EEG signal's fractal properties, show the complexity and irregularity of the signals [21]. Moreover, statistical time-domain features are widely used and in EEG signal processing, present the amplitude and distribution of the signal by encapsulating its statistical properties [17]. Various STD features, comprising minimum, maximum, mean, standard deviation (std), variance (var), and skewness (skew) are extracted from each subband of the approximation coefficients. Therefore, a total of 24 eigenvalue features for each class (Preictal, Ictal) for binary classification and (Preictal, interictal, and ictal) for multi-class classification are extracted. The mathematical expressions for all STD features in this study are given below.

$$Max = max(X) \tag{4}$$

$$Min = min(X) \tag{5}$$

$$Mean = \frac{1}{X} \sum_{i=1}^{X} x_i \tag{6}$$

where X is the total number of values, and x_i are the individual data points.

$$Std = \sqrt{\frac{1}{X - 1} \sum_{i=1}^{X} (x_i - \text{Mean})^2}$$
 (7)

$$Var = \frac{1}{X - 1} \sum_{i=1}^{X} (x_i - Mean)^2$$
 (8)

$$Skew = \frac{1}{N} \sum_{i=1}^{N} \left(\frac{x_i - Mean}{Std} \right)^3$$
 (9)

The features extracted from each subband encompass several measures, including the Katz Fractal Dimension (KFD), Petrosian Fractal Dimension (PFD), Detrended Fluctuation Analysis (DFA), Shannon Entropy (SE), Higuchi Fractal Dimension (HFD), and Hurst (HE), resulting in a total of 12 features. The detailed explanations and mathematical formulations of the fractal dimensions and entropy-based measures can be found in existing literature [17, 18]. The FD-NL features are as follows:

$$KFD = \frac{\log_{10}(n)}{\log_{10}(d/L + 1)}$$
(10)

where n is the total number of points in the time series, d is the Euclidean distance, and L is the total length of the time series.

PFD =
$$\log_{10}(N) / \left(\log_{10}(N) + \log_{10} \left(\frac{N}{N + 0.4N_{\Delta}} \right) \right)$$
 (11)

Where n is the total number of points in the time series and n $N_{-}\Delta n$ is the number of sign changes in the binary sequence.

$$SE = -\sum_{i=1}^{N} P(x_i) \log_2 P(x_i)$$
 (12)

while $P(x_i)$ is the probability of a given value x_i occurring in the time series.

$$HFD = \frac{\log_{10}(L(k))}{\log_{10}(1/k)}$$
 (13)

where L(k) is the length of the time series for a given k and the slope is estimated over a range of k values. Moreover, DFA and HE metrics are often used to evaluate the similarity and long-range temporal correlations in a time series.

To compute DFA the integrated time series Y(k) from the original time series X(i), where i = 1, 2, ..., n:

$$Y(k) = \sum_{i=1}^{k} [X(i) - X_{avg}]$$
 (14)

where X_{avg} is the average of X(i). After, divide Y(k) into N non-overlapping intervals of equal length n. In each interval fit Y(k) (in that interval) with a least squares line fit (k). The fluctuation F(n) is then computed by averaging the residuals from all intervals and then taking the square root:

$$F(n) = \sqrt{\frac{1}{N} \sum_{\nu=1}^{N} \sum_{k=1}^{n} [Y((\nu - 1)n + k) - Y_{\nu}(k)]^2}$$
 (15)

The procedure is repeated for all time scales (window sizes) n to provide a relationship between F(n) and the window size n. The fluctuations can be related to the size of the window by a power law:

$$F(n) \propto n^H \tag{16}$$

After extracting features from the selected decomposition level are passed through feature selection methods, which are discussed in the next section.

Algorithm 2 Feature Extraction Methods

function Signal($E_s, k0, F_S, D_L, w_{size}, over_{siz}$)

2: Load E_s and initialize epoch k = 0

Initialize feature vector FV as an empty list

4: **for** each w_{size} and w_{over} **do**

while $k \ge 0$ do

6: **for** each signal S in E_S and level L in D_L **do**

Decompose S using Wavelet Transform (WT) at level L

8: Extract FD-Nonlinear features

Extract Time-Domain Statistical (TDs) features

10: end for

Append feature vector to FV

12: Evaluate performance using various Feature Metrics (FM)

Increment epoch: k + +

14: end while

Apply dimensional reduction to FV

16: end for

return distinguishable feature vector FV of EEG signals

- 18: end function
- 3.6. Feature selection methods
- 3.6.1. Correlation Coefficient Analysis (CCA) and p-values

To present the relationships between variables, we applied Pearson correlation (PC), which yields values ranging between -1 (indicating a strong negative relationship) and 1 (indicating a strong positive relationship), while the *p*-value substantiates the statistical significance of the experimental results [14]. The feature data consists

of n paired data points, and the PC, denoted as r_{xy} given below:

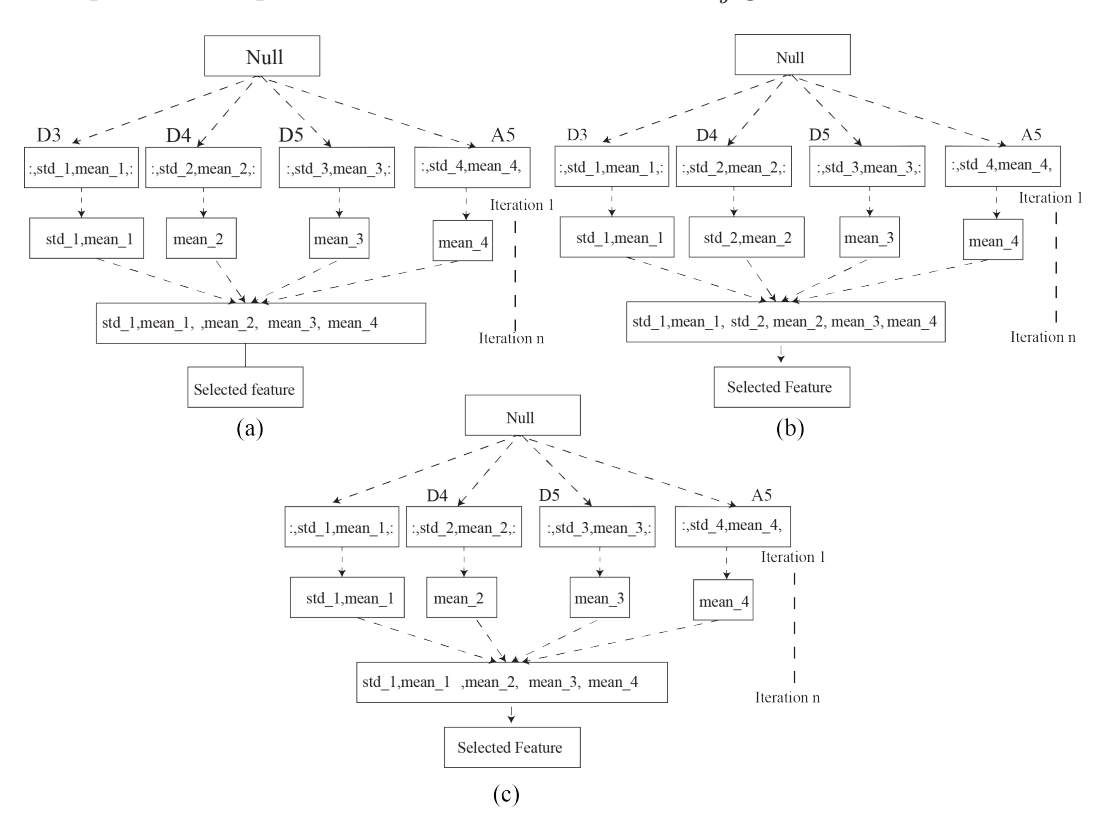


Figure 5: The block diagram of coefficient correlation. (a)(b) Bonn, (c) UCI-EEG dataset

$$r_{xy} = \frac{\sum_{i=1}^{n} (x_i - \bar{x})(y_i - \bar{y})}{\sqrt{\sum_{i=1}^{n} (x_i - \bar{x})^2 \sum_{i=1}^{n} (y_i - \bar{y})^2}}$$
(17)

The x_i and y_i represent individual sample points with index i, while \bar{x} and \bar{y} denote the means of variables x and y respectively, and n symbolizes the total number of data points, the summation symbol $\sum_{i=1}^{n}$ signifies the sum over all n data points. In addition, several experiments are conducted to find the optimal Correlation Coefficient (CC) is 0.8. Features exhibiting correlation above this CC threshold are excluded. Moreover, for feature importance, Null Hypothesis Significance Testing (NHST) is applied, introducing a hypothesis that "no relationship between the se-

lected combination of features and the independent variable". An alpha value of 0.05 is defined, signifying that the null hypothesis is true. The comprehensive overview of mathematical computing of the correlation coefficient is shown in Algorithm 3.

Algorithm 3 Feature Selection via Correlation Coefficient and P-Values

```
1: function Correlation, B_ELIMINATION(Data matrix X, Target vector y, Sig-
    nificance level \alpha)
       Compute the correlation matrix C of X
 2:
       for each pair of features (i, j) do
 3:
           if C_{i,j} \geq 0.8 then
 4:
              Remove one feature from the pair
 5:
           end if
 6:
       end for
 7:
       Define the initial feature subset as NULL
 8:
       while Not all features f are evaluated do
 9:
           Compute p-values for remaining features f relative to target y
10:
           for each feature f do
11:
              if p-value of f < \alpha then
12:
                  Remove feature f
13:
              end if
14:
           end for
15:
           f \leftarrow \text{remaining features}
16:
       end while
17:
18: end function
```

Figure 6 displays the distribution of the selected features following the initial elimination. In the next elimination process, different time-domain (STD) features

are selected for various cases and datasets. In the case (CD-E) from the Bonn dataset, four STD features were chosen mean_3, mean_2, mean_1, and std_1. Similarly, in the case (AB, CD, E), five STD features are selected: mean_3, mean_2, mean_1, std_1, and std_2. Finally, in the case (A, B) from the UCI-EEG dataset, three STD features are selected: mean_3, mean_2, and mean_1. A detailed description of the selected features and their respective decomposition levels is presented in Table 1.

3.6.2. Distance correlation

300

The distance correlation is utilized to manage the variability of feature values, predominantly for nonlinear features. The distance correlation analysis applied in the proposed study includes four steps as follows.

3.6.3. A) Compute Pairwise Distances

Let $U = \{u_1, u_2, \dots, u_n\}$ and $V = \{v_1, v_2, \dots, v_n\}$ represent the feature data for two random variables at each decomposition level feature. First, the pairwise distance matrices, M and N for U and V, respectively, are computed. For a one-dimensional data set, the absolute difference between the elements is given below:

$$M_{ij} = |u_i - u_j|, N_{ij} = |v_i - v_j|$$
(18)

3.6.4. B) Compute double-centered distance matrices

The double-centered distance matrices, M^* and N^* , are derived from M and N^* respectively as follows:

$$M_{ij}^* = M_{ij} - \frac{1}{n} \sum_{k=1}^n M_{ik} - \frac{1}{n} \sum_{k=1}^n M_{kj} + \frac{1}{n^2} \sum_{k=1}^n \sum_{l=1}^n M_{kl},$$
 (19)

$$N_{ij}^* = N_{ij} - \frac{1}{n} \sum_{k=1}^n N_{ik} - \frac{1}{n} \sum_{k=1}^n N_{kj} + \frac{1}{n^2} \sum_{k=1}^n \sum_{l=1}^n N_{kl}$$
 (20)

where M_{ij} and N_{ij} represent the pairwise distances and n indicates the total number of observations.

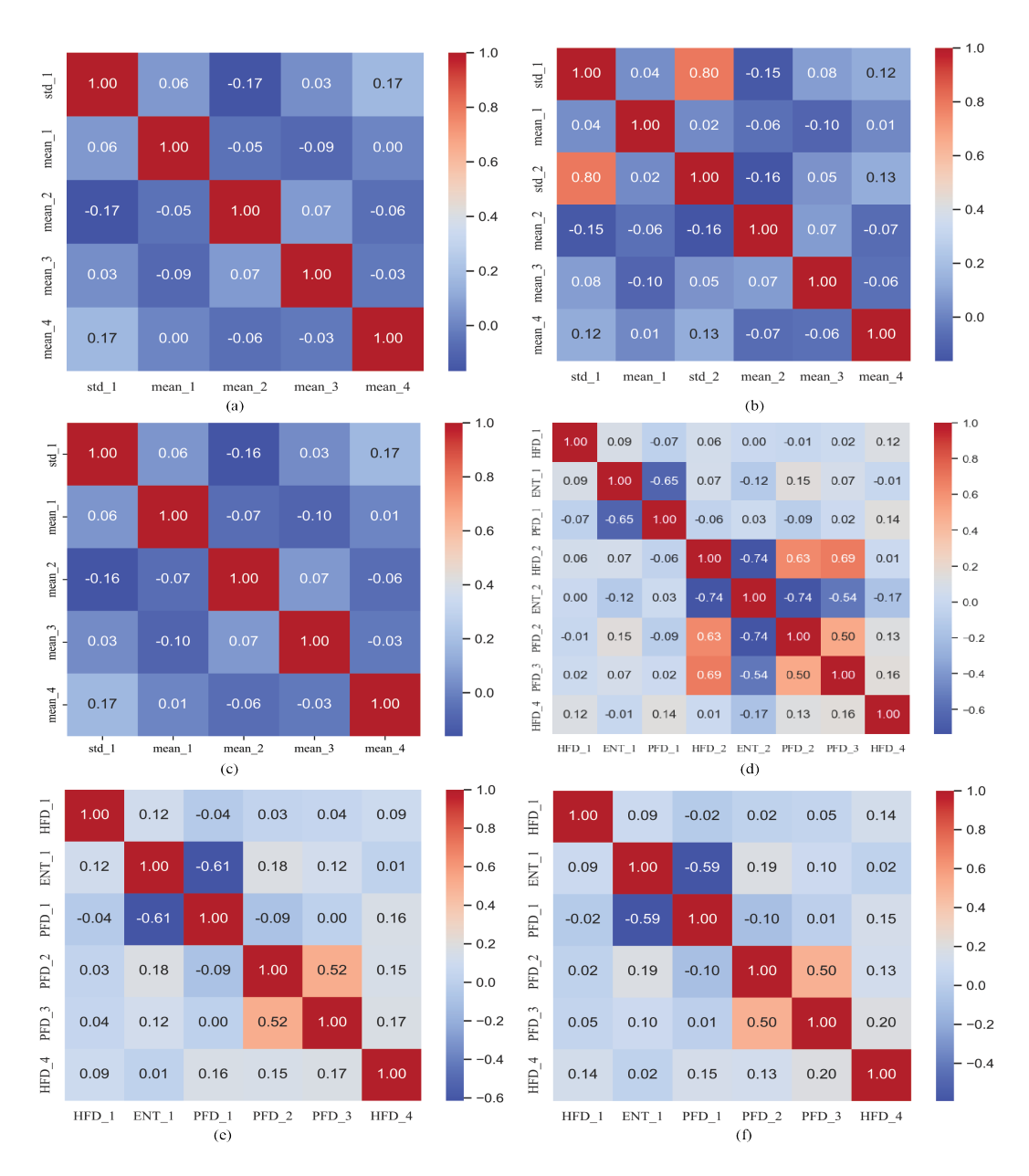


Figure 6: The Correlation coefficient and distance correlation matrix after elimination of highly correlated features. (a)(b)(d)(e) Bonn ,(c)(f) UCI- EEG dataset

3.6.5. C) Calculate distance variances

The distance variance, V(U, U), for a variable U is computed as follows:

$$V(U,U) = \frac{1}{n^2} \sum_{i=1}^{n} \sum_{j=1}^{n} (M_{ij}^*)^2$$
(21)

Similarly, the distance variance, V(V, V), for V is:

$$V(V,V) = \frac{1}{n^2} \sum_{i=1}^{n} \sum_{j=1}^{n} (N_{ij}^*)^2$$
(22)

3.6.6. D) Calculate distance correlation

The distance correlation, R(U, V), is calculated as the square root of the distance covariance normalized by the square root of the product of the distance variances:

$$R(U,V) = \sqrt{\frac{V(U,V)}{\sqrt{V(U,U)V(V,V)}}}$$
(23)

The values of R(U, V) range between 0 and 1, with 0 signifying complete independence between variables, and 1 indicating perfect dependence. Various distance correlation values is used to identify highly correlated features, and performance was assessed post-elimination, employing an optimal distance correlation value of 0.7 for elimination. Figure 6 displays the distribution of the selected features after elimination.

After the elimination process, seven FD-NL features (HFD_4, PF_3, PFD_2, ENT_2, HFD_1, HFD_2, ENT_1) from the case (AB, CD, E) and 5 FD-NL features (HFD_2, PFD_1, ENT_1, ENT_2) from the Bonn dataset were selected, while 5 FD-NL features (HFD_4, PFD_3, PFD_2, PFD_1, ENT_1) from case (A, B) of the UCI-EEG dataset. Figure 7 illustrates the comprehensive process of distance correlation while the descriptions and decomposition levels of the selected features are shown in Table 1.

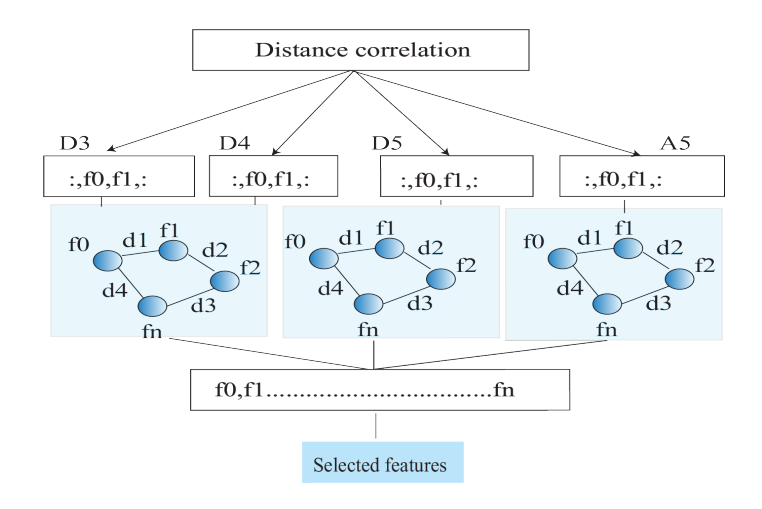


Figure 7: The block diagram of distance correlation.

3.7. Classification model

335

3.7.1. Proposed Bagged Tree-based classifier

In this subsection, the proposed model is explained in detail. The Bonn and the UCI-EEG datasets are highly imbalanced and consist of fewer seizure or ictal samples than non-seizure or preictal instances. So, therefore, the imbalanced feature data created has the potential to bias the model towards over-fitting of the model [5, 26, 27]. To address this issue, we employ a bagging technique with a decision tree in the proposed study. A Bagged Tree-based classifier model manually implements the bagging mechanism to efficiently differentiate different EEG states, especially the inter-class variation [29] and is distinct from a conventional random forest model. Moreover, the bagging mechanism utilizes different individual decision trees to independently classify each feature data bootstrap and then aggregates the outcomes through a voting process to determine the final result, as detailed in Algorithm 4.

The proposed model has three main steps to perform the classification process;

Algorithm 4 Bagging Tree-based Classifier

- 2: Output: Tree-based classifier E
- 3: for $b \leftarrow 1$ to B do
- 4: Sample D_b from D with replacement
- 5: Train base classifier C_b on D_b
- 6: end for
- 7: **function** EnsemblePredict(x)
- 8: $votes \leftarrow \{0, 0, ..., 0\}$
- 9: for $b \leftarrow 1$ to B do
- 10: $c \leftarrow \text{PREDICT}(C_b, x)$
- 11: $votes[c] \leftarrow votes[c] + 1$
- 12: end for
- 13: **return** ARGMAX(votes)

14:

Step 1: Data Input

The enhanced Bagged Tree-based classifier model takes as input feature data represented as D. The dataset encompasses various STD linear and Fractal Dimension (FD) based nonlinear features. The model also requires the number of bootstrap samples B and employs a decision tree as the base classifier C.

Step 2: Bootstrap sampling and model training

In the bootstraps of the proposed model, for each of the B bootstrap samples, a distinct subset D_b is derived from D, with variable sample sizes promoting diversity among samples. This subset is selected with replacement, allowing some instances to repeat, while others may be excluded. Each decision tree C_b is trained on its respective D_b , focusing on optimal splits that minimize the target variable's heterogeneity in the child nodes. The training process continues until it meets a predefined stopping criterion. The process of this step is a collection of B decision trees, each adapted to a uniquely composed feature data set, as shown in Table 5.

Step 3: Prediction function

The function EnsemblePredict(x) in the proposed model is designed for making predictions on new data points x. This function operates by initializing an array of votes for storing class votes. Each tree C_b in the ensemble contributes to the prediction for x, with its vote being weighted based on its accuracy, refining the traditional majority voting mechanism. The class accumulating the highest weighted vote count is then selected as the prediction for x. The proposed model, with its emphasis on customized bagging and weighted voting, offers advantages such as enhanced handling of high-dimensional data, improved robustness against overfitting, and the ability to model complex, non-linear relationships. Additionally, it provides valuable insights into feature importance, aiding in identifying key predictors for seizure occurrences in EEG data.

Table 5: The hyper-parameters for the proposed model in EEG ES detection.

Model	Hyperparameter search space
proposed	$n_estimator = 100, \ max_features = sqrt, \ max_depth = 10,$
model	$min_samples_split = 5, min_samples_leaf = 10, bootstrap =$
	$True, n_jobs = -1, class_weight = balanced, random_state = 42$

4. Explainable Artificial Intelligence (XAI)

In this section, we discuss the interoperability of the proposed model output. XAI helps by offering insights into the AI model's decision-making process. It allows medical experts to validate the model's predictions and make more informed and reliable decisions regarding patient diagnosis and treatment [9, 10]. Moreover, it makes the decision more understandable so that even non-experts or family members of the patients can easily understand the decision, as shown in Figure 1. Recent studies in machine learning (ML) for biomedical signal analysis highlight the urgent need to make their outputs comprehensible. This has led to the rise of Explainable Artificial Intelligence (XAI) systems in smart healthcare systems [10]. Although ML models tend to be more interpretable than deep learning models because of their explainable structure, achieving full interpretability in stacking classifiers remains a challenge. The proposed model employs XAI techniques to elucidate its decision-making processes, feature importance, and inherent biases. Some of the recent XAI methods from the literature are detailed below:

- A) Text Explanations: These provide relevance scores to variables, offering deeper insights.
- B) Local Explanations: This involves understanding the model's responses to minor input changes.

- C) Representative Explanations: Assesses how training data influences decision-making .
- D) Visual Explanations: The specific decision trees that inform outcomes. By
 leveraging the SHAP (Shapley Additive exPlanations) method [10], we highlight the
 individual feature contributions that shape our model's decisions.

5. Experimental Results

This section provides the experimental setup, presents an empirical analysis of the experimental results, and provides an interpretation and explanation of the proposed model's classification performance in the proposed framework.

5.1. Experimental setup

The proposed framework has been experimentally executed using a system configured with a central processing unit (CPU), an NVIDIA Jetson Nano Developer Kit GPU, and a Windows 10 (64-bit) operating system. The system utilizes Python 3.7 within a notebook environment, incorporating libraries such as TensorFlow, Py-EEG, Pandas, Keras, NumPy, and Scikit-Learn. The experiments were conducted on the Bonn and UCI EEG datasets [17, 27]. Various machine learning (ML) models, including RF, LR, DT, XGB, and NB, were employed to assess the performance of the proposed model in EEG epileptic seizure (ES) detection in binary and multiclassification tasks. The configuration and execution settings for the proposed model were constant across all experimental cases and are detailed in Table 5.

In this study, two significant cases from the Bonn dataset are used for binary and multi-classification problems related to EEG ES detection: sets (CD, E) and (AB, CD, E). In the proposed study the data were split 70% for training and 30% for testing. In order to address the limitations of a small dataset, data segmentation

is performed. Moreover, the classification performance of each ML model is evaluated using various performance metrics, such as accuracy (ACC), precision (PR), sensitivity (SE), specificity (SP), and the F1-score (F1) [25, 26].

$$ACC(\%) = \frac{T_{Positive} + T_{Negative}}{N}$$
 (24)

Where, $N = T_{Positive} + T_{Negative} + F_{Positive} + F_{Negative}$

420

$$PR(\%) = \frac{T_{Positive}}{T_{Positive} + F_{Positive}}$$
 (25)

 $RE(\%) = \frac{T_{Positive}}{T_{Positive} + F_{Negative}}$ (26)

$$SP(\%) = \frac{T_{Negative}}{T - Neagtive + F_{Positive}}$$
 (27)

$$F1 = 2 * \frac{RE * PR}{RE + PR} \tag{28}$$

where TP, TN, FP, and FN denote the total number of correctly detected positives (seizure), correctly detected negatives (non-seizure), incorrectly identified positives, and incorrectly identified negatives, respectively.

5.2. The time complexity of the feature extraction methods

In the process of feature extraction, different wavelet features, as mentioned in subsection 3.5 are extracted from DWT sub-bands. Moreover, the execution time of the feature plays an important role in rule-based hardware implementation. The study also examines the feature extraction time of the method in the experiment. Figure 8 shows the execution time of the features. The execution times are repeated in different experimental cases, therefore, we select the average of the time complexities. All the features have less time as compared to the relevant literature [16, 17, 18].

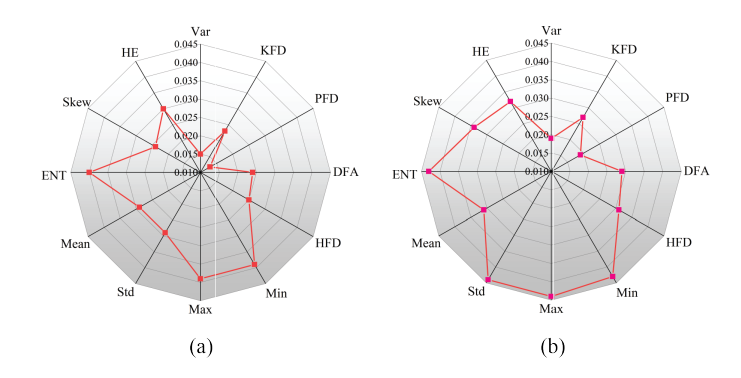


Figure 8: The execution time of the feature. (a) Bonn dataset, (b) UCI-EEG dataset.

5.3. Analysis and performance of different coefficient and distance correlation measure

This subsection empirically evaluates the optimal features mentioned in subsections 3.6.1 and 3.6.2. The approach uses two cases from the Bonn EEG dataset and one from the UCI- EEG dataset, with varying correlation coefficient (CC) values (0.5, 0.6, 0.7, 0.8, and 0.9) to determine their respective accuracies (%).

Figure 10 (a) illustrates that accuracy increases when the CC value reaches 0.8. Beyond the 0.8 threshold value, the average accuracy across experiments is constant. Specifically, at CC = 0.8, the case (CD, E) from the Bonn EEG dataset, utilizing features provided in subsection 3.6.1 shows a maximum accuracy of 98.6%. Similarly, the case (AB, CD, E), incorporating features mentioned in subsection 3.6.1, reports an equivalent accuracy.

In Figure 10 (b), a similar performance is observed up to CC = 0.9 for the UCI-EEG dataset. Across all experiments involving different CC, the p-values remained constant at 0.005 during the second elimination. Moreover, the proposed selected feature of the STD from cases (A, B) yielded the highest binary EEG epileptic seizure (ES) detection accuracy of 98.3%.

Figure 10 (c)(d) depicts the performance for non-linear feature selection from wavelet decomposition using distance correlation (DC). The accuracy increases until DC = 0.7, subsequently stabilizing. At DC = 0.8 and DC = 0.9, the optimal non-linear features from subsection 3.6.2, applied to the case (AB, CD, E), achieve a peak accuracy of 97.2%. For case (CD, E), features selected from subsection 3.6.2 realize an accuracy of 97.08%. A parallel process is observed for the UCI-EEG dataset, where features from subsection 3.6.2 at DC = 0.7 from the case (AB, CD, E), show the maximum accuracy up to 98.2%.

5.4. Ablation study

475

In this subsection, the performance of the proposed model for EEG epileptic seizure detection is analyzed. The over-fitting of the model is illustrated through training Vs testing accuracy and training loss Vs testing loss with respect to the number of trees, as shown in Figure 11, With effective learning from the optimal linear and non-linear features, the model achieved a training accuracy of 98.2% and a loss of 0.07%, whereas the validation accuracy reached 98.10% with a loss of 0.08% after employing 60 trees. As the number of trees increases, the model progressively enhances the accuracy and reduces the loss to 0.08%, given that the bagged techniques handle the over-fitting issue efficiently. The performance of the model shows that the number of trees increased to 50, with the performance accuracy of the proposed model also increasing. After the number of trees increases, it has no effect on the model's performance. Initially. The same process is repeated for the loss of the proposed model.

5.5. Experimental analysis and performance of the proposed model

In this subsection, we discuss the comprehensive results of the proposed model. Initially, the Receiver Operating Characteristic (ROC) curve is utilized to evaluate

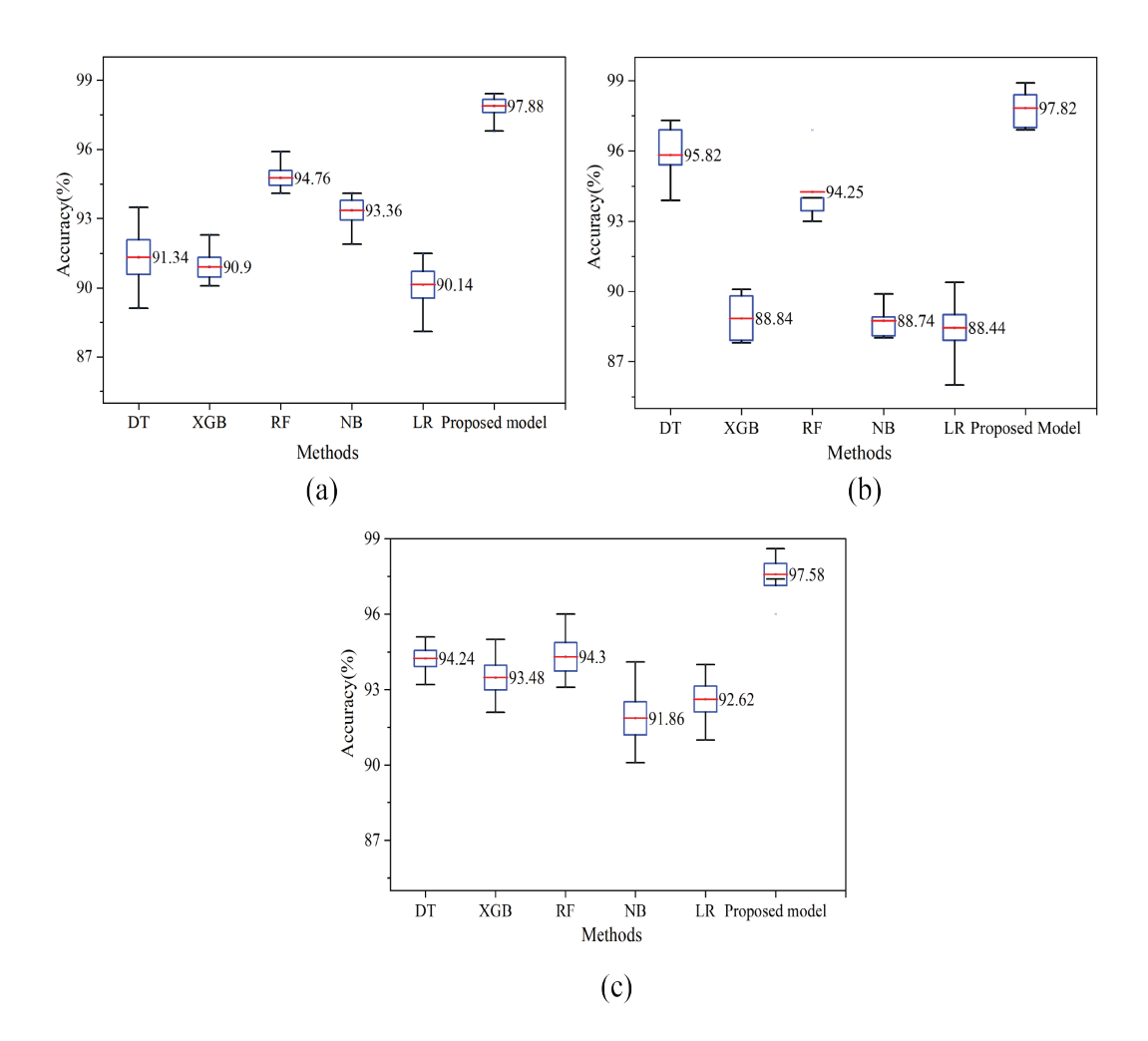


Figure 9: Comparative results of the proposed model with recent ML models. (a)(b) Bonn ,(c) UCI-EEG EEG dataset data set.

the model's efficiency, as shown in Figure 13 which presents the ROC curve of the proposed classifier, derived from various EEG class detection systems, indicating that the proposed model achieved averages of 0.99 and 1.00, respectively. Moreover, we also discuss the extended indicators of performance, including the False Detection Rate (FDR), False Omission Rate (FOR), False Positive Rate (FPR), and False Negative Rate (FNR). Furthermore, Figure 12 shows the superior performance of

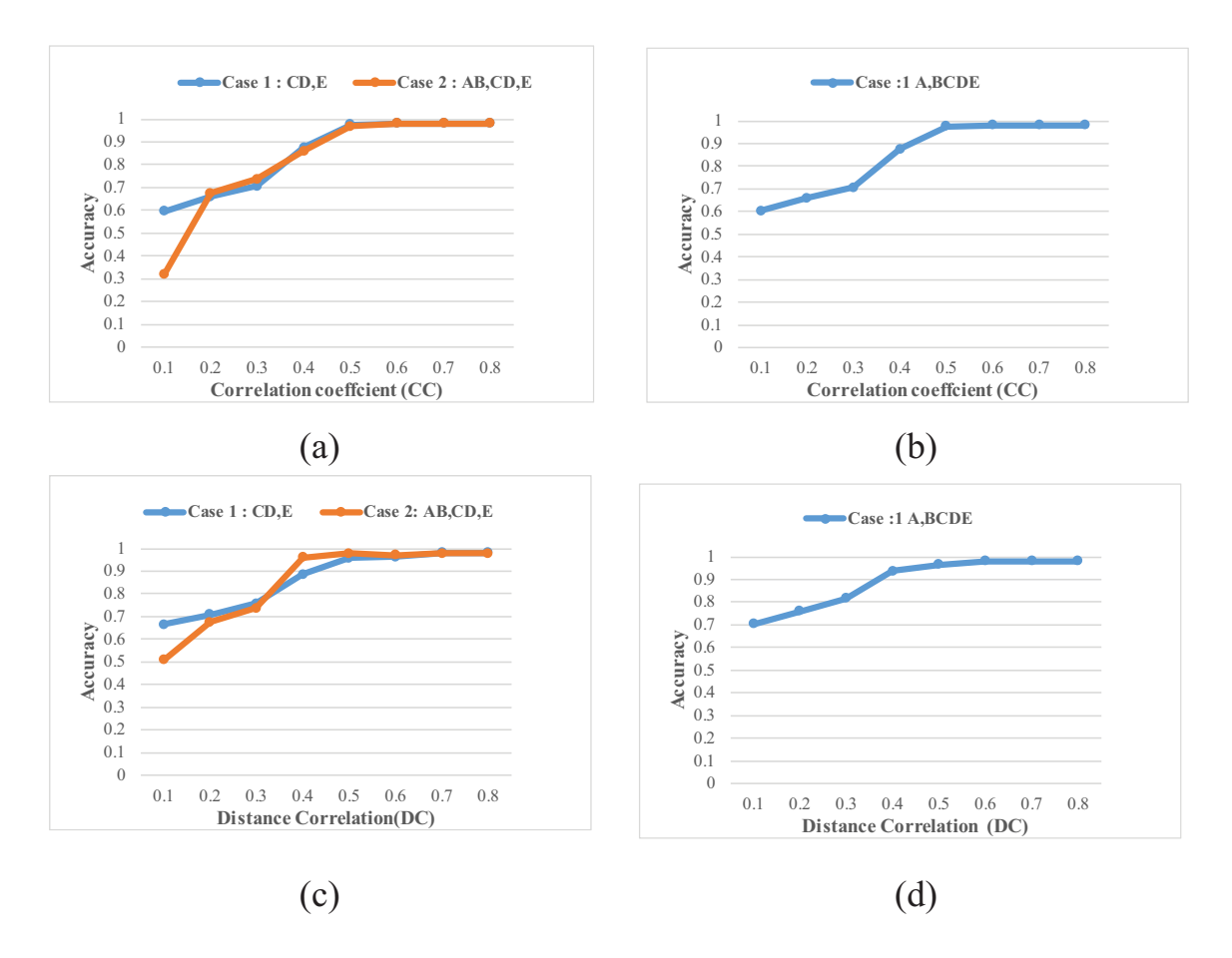


Figure 10: Correlation coefficient and distance correlation-based accuracy. (a)(c) Bonn dataset, (b)(d) UCI-EEG dataset.

the proposed model, achieving average rates of FDR (0.0268%), FPR (0.0356%), FOR (0.0159%), and FNR (0.011%) across both cases using the Bonn dataset. In the case of the UCI-EEG dataset, the model demonstrates the FDR of 0.0278%, FPR of 0.0213%, FOR of 0.0341%, and FNR of 0.0245% for binary classification tasks in EEG epileptic seizure detection.

Additionally, Table 6 presents the average computation time for each case using [18, 20, 21, 22], which shows the proposed model is time-efficient.

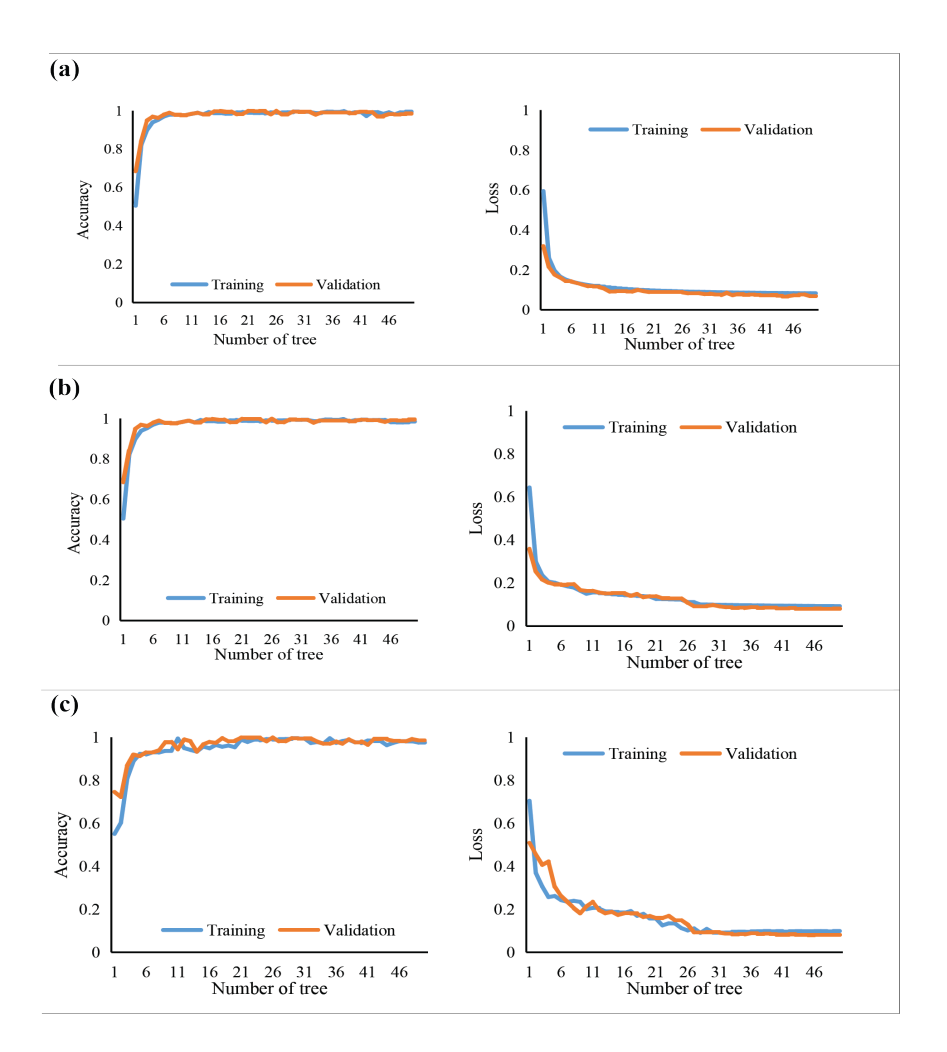


Figure 11: Average accuracy vs average loss with respect to the number of trees. (a)(b) experimental analysis of the training process of the proposed model using the Bonn EEG dataset, (c) UCI-EEG dataset models.

5.6. Empirical analysis of the proposed framework features and models

This subsection discusses a comparative performance analysis between the proposed model and various machine learning models LR, XGB, DT, NB, and RF using optimal linear and non-linear features using two data selection methods including 5-fold cross-validation and holdout (70% training, 30% testing) methods. Figure 9

Table 6: The computational time of the proposed framework in EEG ES detection.

Progress	Time (sec)
Pre-processing	4
DWT	10.40
Feature extraction	12.10
Classification	10.03

Figure 9(a) and (b) highlight that the proposed model, employing optimal features, achieved the highest mean accuracy. For the Bonn EEG dataset, mean accuracies are 97.88% and 97.82% for cases (CD-E) and (AB, CD, E) respectively in EEG ES detection, while NB reported the lowest mean accuracy. Furthermore, Figure 9 (c) indicates the proposed model archived the highest mean accuracy, 97.58%, for the UCI case (A, B), with the NB model yielding the lowest performance.

Moreover, Tables 9 and 10 present the performance of the proposed model with other ML classifiers using 70% training data and 30% for testing. The proposed model, utilizing a combination of STD and FD-NL, achieved the best performance using the experimental case (CD, E) from the Bonn EEG dataset having an accuracy of 99.50%, precision of 98.42%, sensitivity of 98.42%, specificity of 98.40%, and F1-score 98.40%. Moreover, in the case (AB, CD, E) of the boon EEG data set the proposed model achieved 99.50% accuracy, 98.40% precision, 98.30% sensitivity, 98.40% specificity, and 98.40% F1-score. For (A, B) from the UCI-EEG, the model reported 99.60% accuracy, 99.50% precision, 99.40% sensitivity, 99.40% specificity, and 99.15% F1-score, while the (A, B) from the combination set from the UCI-EEG dataset, as shown in Table 10, the proposed classifier outperformed other machine

learning models On the other hand, the LR had the lowest performance among all the models.

Table 7: The experimental results of the proposed model with other sibling ML models using Bonn EEG data set.

Methods	Sets	ACC (%)	PR(%)	RE(%)	SP(%)	F1(%)
DIT	(CD,E)	96.67	96.50	96.50	96.40	96.40
DT	$\overline{\text{(AB,CD,E)}}$	97.10	97.10	97.00	97.70	97.05
VCD	(CD, E)	94.49	94.50	94.43	94.10	94.30
XGB	$\overline{\text{(AB,CD,E)}}$	92.80	92.80	92.60	92.50	91.65
DE	(CD,E)	95.49	95.10	94.50	94	94.30
RF	(AB,CD,E)	92.90	92.40	92.10	91.40	91.90
ND	(CD,E)	94.30	93.80	93.80	93.70	94.10
NB	$\overline{\text{(AB,CD,E)}}$	93.20	92.80	92.20	92.10	93.20
I D	(CD,E)	93.07	92.20	92.10	92.05	93.01
LR	(AB,CD,E)	93.60	93.30	93.20	92.90	93.60
Dropogod model	(CD,E)	99.50	98.42	98.40	98.42	98.40
Proposed model	(AB,CD,E)	99.50	98.40	98.30	98.40	98.40

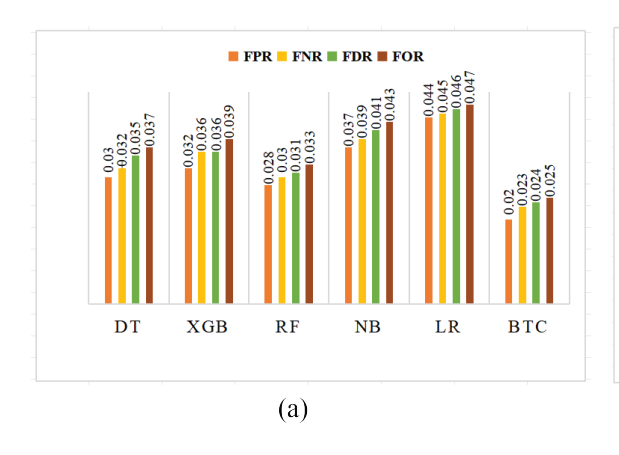
Table 8: Experimental results of the proposed model with other sibling ML models using UCI-EEG dataset.

Methods	Sets	ACC (%)	PR(%)	RE(%)	SP(%)	F1(%)
RF	(A,B)	97.10	97.05	97.00	96.80	96.90
XGB	(A,B-E)	97.80	96.59	96.10	96.00	96.90
DT	(A,B)	97.90	97.80	97.00	96.90	97.10
NB	(A,B)	94.50	94.10	93.00	93.90	93.60
LR	(A,B)	94.23	93.40	93.40	93.10	93.20
Proposed	(A,B-E)	99.60	99.50	99.40	99.40	99.50
model						

$_{15}$ 5.7. Interpretability and Explainability of the proposed model using XAI

In this subsection, we explain the interpretation of all the performance of experimental cases in each dataset through Explainable AI (XAI). We used SHAP (SHapley Additive exPlanations), a game theory approach, to explain the decision-making process of the models, as demonstrated by the various SHAP decision plots. These visualizations include the Summary Plot (SP) and Waterfall Plot (WP). The SP plot is illustrated in Figure 14 (a) (b) and Figure 15 (a) providing a global interpretation of the model of Bonn and UCI-EEG dataset of different cases.

The plot shows the feature's importance with respect to classification performance, revealing the influence of each global feature on the model's outcome. The eigenvalue feature HFD₄ with large absolute SVs is identified as significant due to their higher average impact on the model's output. Figure 14 (c) (d) and 15 (b)



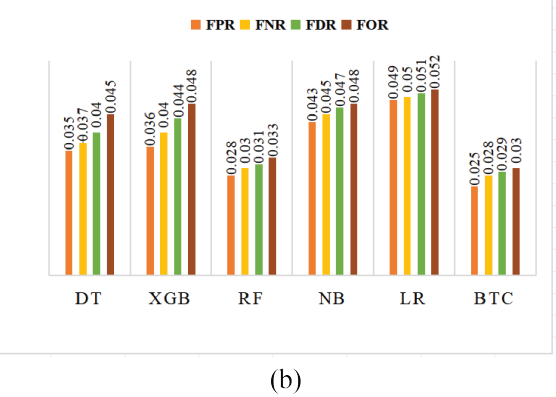


Figure 12: The analysis based on FDR, FNR, FOR, and FPR of the proposed model in EEG epileptic seizure detection. (a) Bonn, (b) UCI-EEG data set.

shows the WP plot for the Bonn and UCI cases, highlights the behavior of True Positives (TP), False Positives (FP), False Negatives (FN), and True Negatives (TN). The WP plot uses red and blue bars to indicate features that contribute to the overall classification score, with the ability to either decrease or increase the score. Moreover, Figure 16 (a) to (d), presents the SHAP dependence plot which describes the relationship between two eigenvalue features of the STD and FD-NL and the effect on their model performance. In the plot, the x-axis represents the primary feature while the y-axis on the left side represents the secondary feature and the y-axis on the right side represents the Shape values. In plots (a), (b), (c), (d), the primary and secondary features across multiple domains show an increase as the shape value increases, indicating a positive correlation with the predicted outcome. Through these visualizations, it becomes evident that HFD-4 plays the most significant role in distinguishing between EEG states using each dataset, while ENT-1 eigenvalues are the least important in EEG epileptic seizure detection.

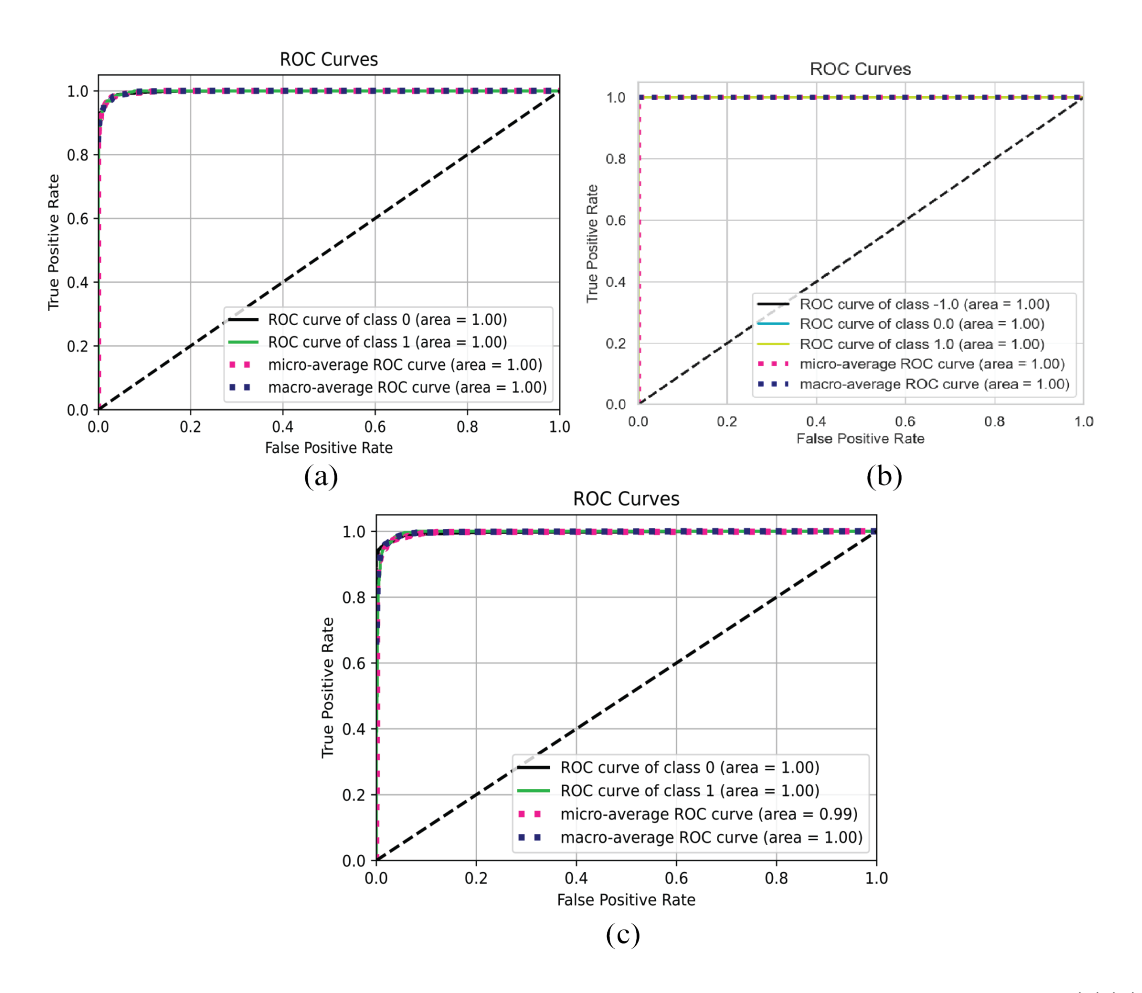


Figure 13: The ROC curve of the proposed model using different combination sets of EEG. (a)(b) Bonn, (c) UCI.

6. Discussion

Epileptic seizure presents significant challenges in healthcare technology. This is primarily due to the complex and non-linear nature of EEG signals, as well as the influence of various factors on seizure activity. Conventional seizure detection methods often fall short of accurately representing the dynamic proposed nature of these signals.

Furthermore, selecting the optimal features for EEG epileptic seizure (ES) de-

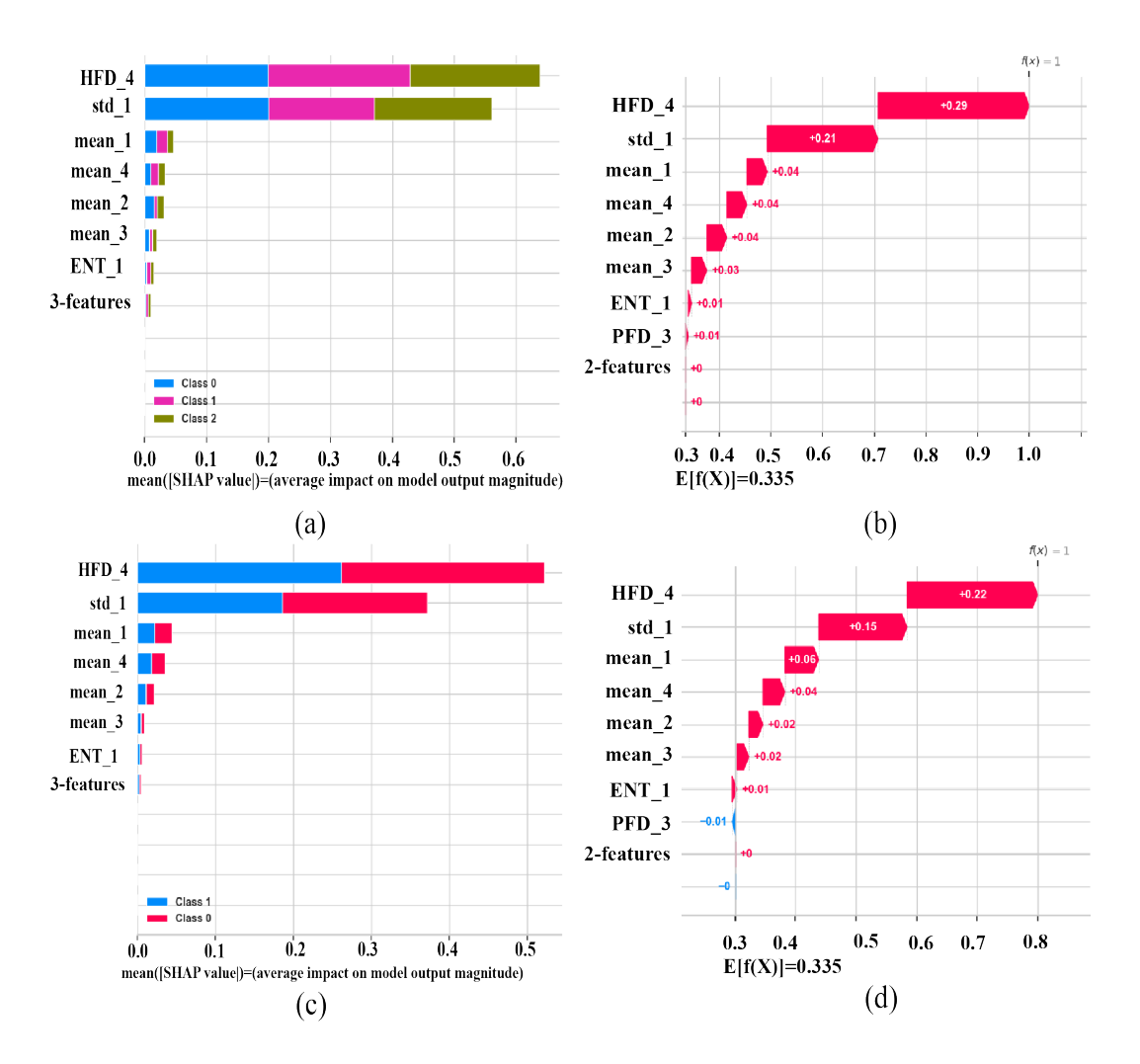


Figure 14: Visual explanations for the proposed model based on different visualizations for binary and multi-class tasks using the Bonn dataset. Subfigures (a) and (c) represent summary plots, while (b) and (d) are waterfall plots.

tection within an automated system poses an additional challenge. The aim is to enhance classification performance by identifying the most informative features. Choosing effective features for use by ML models is essential to improve accuracy and sensitivity in ES detection compared to other methods. Moreover, ensuring model explainability and interpretability in the proposed decision-making process presents

further challenges [30, 31, 32, 33, 34]. To the best of the authors' knowledge, no prior research has employed the correlation coefficient and distance correlation for linear and nonlinear feature selection, the Bagged Tree-based classifier, or explored the model's explainability and interpretability through explainable AI, which includes both global and local explanations.

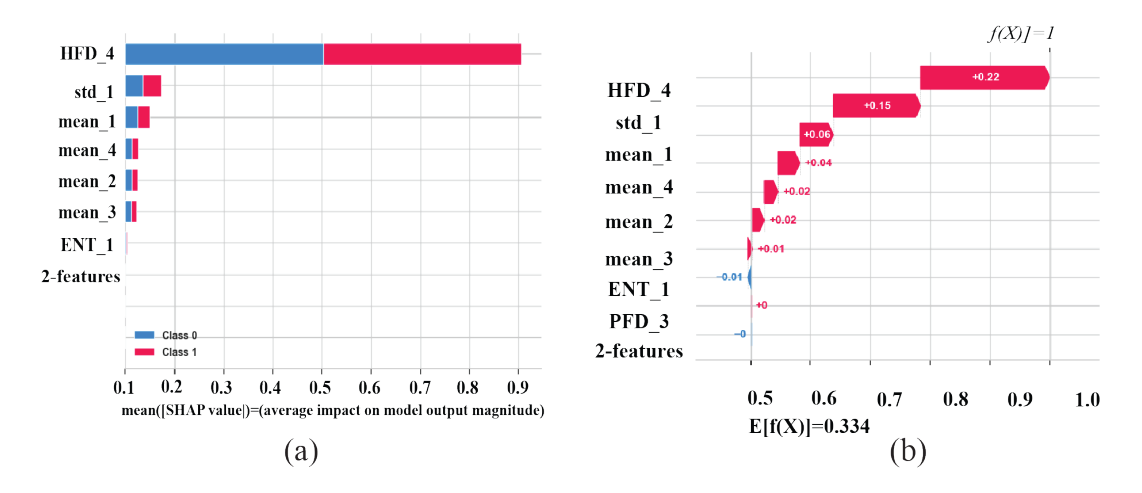


Figure 15: The Explainability of the proposed model performance based on different visualizations for the binary class using the UCI- EEG dataset. Subfigure (a) represents the summary plot, while (b) depicts the waterfall plot.

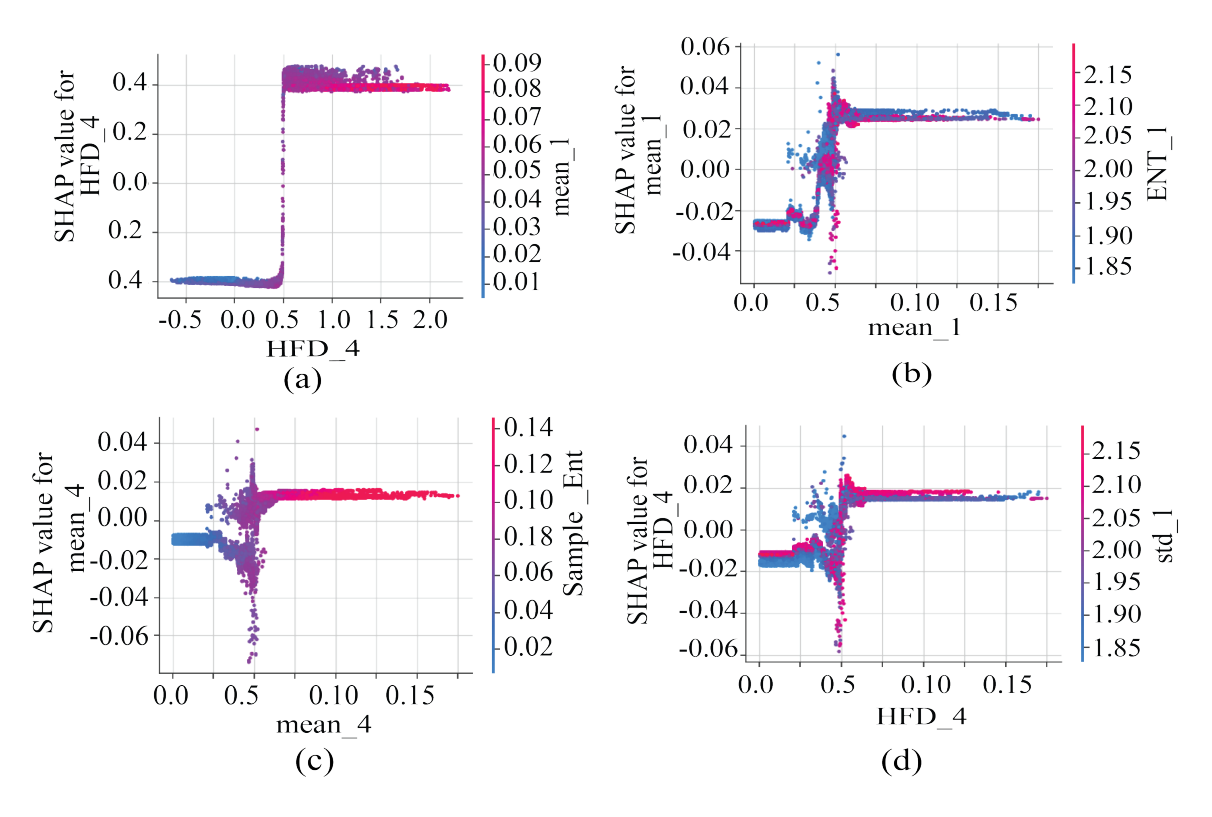


Figure 16: The Dependency plot (a)(b)(c)(d) represents the different primary and secondary features.

Table 9: The comparative results of the proposed model with state-of-the-art methods using the Bonn dataset.

Publ.	Seg,sample	Cases	Methods	Expl.	ACC (%)	Time
						complex-
						ity (%)
[35]	NA,4097	(ABCD,	TQWT +Entropy	NA	99	NA
		E), (AB,	feature+PCA+ SVM			
		CD, E)				
[17]	NA,4097	(C-E), (D-	CWT + Wavelet fea-	NA	97, 96	NA
		E)	tures + SVM,NB			
[36]	NA, 4097	(AB,CD,E)	DTCWT + ST +	NA	98	90
			CVNN			
[37]	NA,4097	(C, E) and	DWT, Windowing+	NA	97	NA
		(D, E)	ST + LSTM			
[38]	NA,4097	(CD,E)	Normalization +	NA	95.16%	NA
			DNN Model			
[39]	NA, 4097	(CD,E)	FLP + PEE, Energy	NA	97.17%	NA
			+ SVM			
This work	69,1008	(CD,E	DWT + STD and	XAI	99.50,	35
),(AB,CD,E)FD-NL, + CC and		99.50	
			DC +			

Exple:Explainability;DTCWT, Dual-tree complex wavelet transform; TQWT, Tunable Q wavelet transform; CVNN, Complex value neural networks; CC, correlation coefficient;DC, distance correlation;ST,statistical features.

4

Table 10: The comparative results of the proposed model with state-of-art methods using the UCI-EEG dataset.

Publ.	Seg,sample	Cases	Methods	Expl.	ACC (%)	Time complex-ity (%)
[40]	Event based	(A,B-E)	FT +178 features +SVM, KNN, ANN	NA	97,96, 95	NA
[41]	Event based	(A,B)	DCPA-EZ + DCPA- EZ	NA	98.10	NA
[42]	Event based	(A,B)	178 features +SVM, KNN, ANN, LDA	Event based	95, 96.40, 93, 94	NA
[43]	Event based	(A, B)	FFT + wavelet fea- tures + SOM-RBFnn	NA	97.40	NA
[44]	Event based	(A,B)	FFT+ 178 features+ NAMLP, ANN, SVM	NA	94, 93, 92	NA
This work	86,1330	(A,B)	DWT + FD-NL,STD features + feature se- lection (CC and DC) +	XAI	99.40	19

Pub: Publication; Exapl, Explainability; DCPA-EZ, deep canonical sparse autoencoder-based epileptic seizure detection; SOM-RBFnn, self-organizing map radial basis function neural network; FFT, Fast Fourier transform.

In addressing the challenges of EEG epileptic seizure detection, the proposed study presents a comprehensive framework that integrates various components, which includes EEG signal decomposition, noise mitigation, statistical time domain (STD), and Fractal Dimension-based (FD) non-linear feature extraction, with innovative feature selection methods. The proposed Bagged Tree-based classifier effectively addresses over-fitting concerns and enhances interpretability through Explainable Artificial Intelligence (XAI).

565

Performance evaluations using the Bonn and UCI-EEG datasets validate the effectiveness of the proposed framework. The results (Figure 10) indicate optimal performance at a correlation coefficient (CC) value of 0.8. Beyond the proposed threshold, even increases in CC did not improve accuracy. Therefore, the CC value of 0.8 serves as the threshold for the model's learning and streamlines feature selection. The proposed framework incorporates FD-based linear and non-linear features extracted through wavelet decomposition. The approach uses both the linear and complex attributes of EEG signals, thereby enhancing the model's discrimination capacity. Comparison with various machine learning models (DT, RF, XGB, LR, NB) via 5-fold cross-validation demonstrates the superior performance of the proposed model. The proposed model consistently outperforms other ML models using the Bonn and UCI-EEG data set showing the effectiveness of the proposed model. The model used the selected non-linear and STD linear features, effectively distinguishing the seizure, non-seizure, and transition EEG states. The proposed model performance is benchmarked against recent state of art methods validated by Bonn and UCI- EEG datasets (Tables 9 and 10), consistently outperformed existing methods, with an average accuracy of 99.50% for Bonn and 99.40% for UCI-EEG dataset.

Explainable AI (XAI) through SHAP presents the interpretation of the proposed model decision-making to medical experts. Summary and Waterfall Plots highlight the important features and their contributions to classifications.

In summary, the proposed methods significantly enhance EEG epileptic seizure detection, not only enhancing the accuracy but also explaining the decision-making process, a key advantage in healthcare settings where understanding model decisions is crucial. The high precision, sensitivity, and accuracy of the proposed framework highlight its potential for healthcare professionals in diagnosing seizures. The comprehensive understanding of EEG signals, improved feature selection through optimized correlation coefficients, robust overfitting management by the model, and transparent decision-making via SHAP collectively contribute to informed decision-making, enhancing patient care and outcomes in epilepsy management, while the proposed framework offers several advantages, it is essential to acknowledge its limitations. The proposed framework is best for the patients specifically. In future studies, our goal is to apply the framework to patient-independent, utilizing larger and more comprehensive clinical datasets.

7. Conclusion

585

In this study, we introduce an automatic EEG epileptic seizure detection framework that applies novel feature selection methods, a Bagged Tree-based classifier, and Explainable Artificial Intelligence (XAI). Initially, the pre-processing of EEG signals using a Butterworth filter to reduce noise and artifacts. Then, discrete wavelet transform (DWT) based decomposition is applied, and statistical time domain linear and FD-nonlinear features are extracted from each decomposition level. The use of a novel correlation coefficient for linear features and distance correlation for non-linear features enables effective feature selection, improving the model's performance in EEG epileptic seizure detection. The model exhibits the best performance metrics in accuracy, precision, and sensitivity, effectively addressing the over-fitting issue.

Validation through Bonn and UCI EEG benchmark datasets confirms the model's robustness and reliability in detecting epileptic seizures. The important aspect of the proposed framework is the incorporation of XAI, achieved through SHapley Additive Explanations (SHAP), which interprets the model's decision-making process, and explains the impact of each feature on the model's output. The future will focus on patient-independent multimodel data using the proposed framework with explainability and interpretability to facilitate the clinical decision-making process in epilepsy management.

Acknowledgements

This work was supported in part by the National Key R& D Program of China (2022YFE0197500), National Natural Science Foundation of China (#81927804, #62101538), Science and Technology Planning Project of Shenzhen (#JSGG2021071 3091808027, #JSGG20211029095801002), China Postdoctoral Science Foundation (2022M710968), the Science and Technology Program of Guangdong Province (2022A 0505090007).

References

- [1] C. Spagnoli, C. Fusco, F. Pisani, Rett syndrome spectrum in monogenic developmental-epileptic encephalopathies and epilepsies: A review, Genes 12 (8) (2021) 1157.
 - [2] S. Pati, A. V. Alexopoulos, Pharmacoresistant epilepsy: from pathogenesis to current and emerging therapies, Cleve Clin J Med 77 (7) (2010) 457–567.
- 630 [3] M. A. Obeidat, A. M. Mansour, Eeg based epilepsy diagnosis system using

- reconstruction phase space and naïve bayes classifier, WSEAS Transactions on Circuits and Systems 17 (2018).
- [4] WHO, Epilepsy care, Availableonline:https://www.who.int/mental_health (2022 (accessed December 7, 2022)).
- [5] A. Subasi, J. Kevric, M. Abdullah Canbaz, Epileptic seizure detection using hybrid machine learning methods, Neural Computing and Applications 31 (2019) 317–325.
 - [6] X. Ijaz Ahmad, Wang, M. Zhu, C. Wang, Y. Pi, J. A. Khan, S. Khan, O. W. Samuel, S. Chen, G. Li, Eeg-based epileptic seizure detection via machine/deep learning approaches: A systematic review, Computational Intelligence and Neuroscience 2022 (2022).

640

- [7] A. S. Abdulbaqi, M. T. Younis, Y. T. Younus, A. J. Obaid, A hybrid technique for eeg signals evaluation and classification as a step towards to neurological and cerebral disorders diagnosis, International Journal of Nonlinear Analysis and Applications 13 (1) (2022) 773–781.
- [8] M. S. Nafea, Z. H. Ismail, Supervised machine learning and deep learning techniques for epileptic seizure recognition using eeg signals—a systematic literature review, Bioengineering 9 (12) (2022) 781.
- [9] E. Tjoa, C. Guan, A survey on explainable artificial intelligence (xai): Toward medical xai, IEEE transactions on neural networks and learning systems 32 (11) (2020) 4793–4813.
 - [10] D. Raab, A. Theissler, M. Spiliopoulou, Xai4eeg: spectral and spatio-temporal

- explanation of deep learning-based seizure detection in eeg time series, Neural Computing and Applications (2022) 1–18.
- [11] W. Al-Salman, Y. Li, P. Wen, F. S. Miften, A. Y. Oudah, H. R. Al Ghayab, Extracting epileptic features in eegs using a dual-tree complex wavelet transform coupled with a classification algorithm, Brain Research 1779 (2022) 147777.
 - [12] G. Kaushik, P. Gaur, R. R. Sharma, R. B. Pachori, Eeg signal based seizure detection focused on hjorth parameters from tunable-q wavelet sub-bands, Biomedical Signal Processing and Control 76 (2022) 103645.

660

- [13] I. M. Nasir, M. A. Khan, M. Yasmin, J. H. Shah, M. Gabryel, R. Scherer, R. Damaševičius, Pearson correlation-based feature selection for document classification using balanced training, Sensors 20 (23) (2020) 6793.
- [14] I. Aliyu, C. G. Lim, Selection of optimal wavelet features for epileptic eeg signal classification with lstm, Neural Computing and Applications (2021) 1–21.
 - [15] R. G. Andrzejak, K. Lehnertz, F. Mormann, C. Rieke, P. David, C. E. Elger, Indications of nonlinear deterministic and finite-dimensional structures in time series of brain electrical activity: Dependence on recording region and brain state, Physical Review E 64 (6) (2001) 061907.
- [16] B. Harender, R. Sharma, Dwt based epileptic seizure detection from eeg signal using k-nn classifier, in: 2017 International Conference on Trends in Electronics and Informatics (ICEI), IEEE, 2017, pp. 762–765.
 - [17] A. Sharmila, P. Geethanjali, Dwt based detection of epileptic seizure from eeg signals using naive bayes and k-nn classifiers, Ieee Access 4 (2016) 7716–7727.

- [18] R. Uthayakumar, D. Easwaramoorthy, Epileptic seizure detection in eeg signals using multifractal analysis and wavelet transform, Fractals 21 (02) (2013) 1350011.
 - [19] T. M. E. Nijsen, Accelerometry based detection of epileptic seizures (2008).
- [20] A. Parashar, A. Parashar, W. Ding, M. Shabaz, Data preprocessing and feature selection techniques in gait recognition: A comparative study of machine learning and deep learning approaches, Pattern Recognition Letters (2023).
 - [21] S. F. Hussain, S. M. Qaisar, Epileptic seizure classification using level-crossing eeg sampling and ensemble of sub-problems classifier, Expert Systems with Applications 191 (2022) 116356.
- [22] L. Xie, Z. Li, Y. Zhou, Y. He, J. Zhu, Computational diagnostic techniques for electrocardiogram signal analysis, Sensors 20 (21) (2020) 6318.
 - [23] A. Nishad, Tunable-q wavelets transform based filter banks for non-stationary signals analysis and classification (2019).
- [24] R. Upadhyay, A. Manglick, D. Reddy, P. Padhy, P. K. Kankar, Channel optimization and nonlinear feature extraction for electroencephalogram signals classification, Computers & Electrical Engineering 45 (2015) 222–234.
 - [25] L. Fei, B. Zhang, Y. Xu, C. Tian, Jointly heterogeneous palmprint discriminant feature learning, IEEE Transactions on Neural Networks and Learning Systems 33 (9) (2021) 4979–4990.
- [26] M. T. Sadiq, X. Yu, Z. Yuan, F. Zeming, A. U. Rehman, I. Ullah, G. Li, G. Xiao, Motor imagery eeg signals decoding by multivariate empirical wavelet transform-

- based framework for robust brain-computer interfaces, IEEE access 7 (2019) 171431–171451.
- [27] U.M.L, Repository, epileptic seizure recognition data set, https://archive.

 ics.uci.edu/ml/datasets/Epileptic+Seizure+Recognition (May 2022).
 - [28] N. Ji, L. Ma, H. Dong, X. Zhang, Eeg signals feature extraction based on dwt and emd combined with approximate entropy, Brain sciences 9 (8) (2019) 201.
 - [29] K. Rasheed, A. Qayyum, J. Qadir, S. Sivathamboo, P. Kwan, L. Kuhlmann, T. O'Brien, A. Razi, Machine learning for predicting epileptic seizures using eeg signals: A review, IEEE Reviews in Biomedical Engineering 14 (2020) 139–155.

- [30] L. Fei, S. Teng, J. Wu, Enhanced minutiae extraction for high-resolution palmprint recognition, International Journal of Image and Graphics 17 (04) (2017) 1750020.
- [31] N. K. Al-Qazzaz, S. H. B. M. Ali, S. A. Ahmad, Recognition enhancement of dementia patients' working memory using entropy-based features and local tangent space alignment algorithm, in: Advances in Non-Invasive Biomedical Signal Sensing and Processing with Machine Learning, Springer, 2023, pp. 345– 373.
- [32] M. Mursalin, Y. Zhang, Y. Chen, N. V. Chawla, Automated epileptic seizure detection using improved correlation-based feature selection with random forest classifier, Neurocomputing 241 (2017) 204–214.
 - [33] B. A. Demirci, O. Demirci, M. Engin, Comparative analysis of ann performance of four feature extraction methods used in the detection of epileptic seizures, Computers in Biology and Medicine (2023) 107491.

- [34] W. Mardini, M. M. B. Yassein, R. Al-Rawashdeh, S. Aljawarneh, Y. Khamay-seh, O. Meqdadi, Enhanced detection of epileptic seizure using eeg signals in combination with machine learning classifiers, IEEE Access 8 (2020) 24046–24055.
- [35] M. Peker, B. Sen, D. Delen, A novel method for automated diagnosis of epilepsy using complex-valued classifiers, IEEE journal of biomedical and health informatics 20 (1) (2015) 108–118.
 - [36] S. Supriya, S. Siuly, H. Wang, J. Cao, Y. Zhang, Weighted visibility graph with complex network features in the detection of epilepsy, IEEE access 4 (2016) 6554–6566.
- [37] K. Akyol, Stacking ensemble based deep neural networks modeling for effective epileptic seizure detection, Expert Systems with Applications 148 (2020) 113239.
 - [38] V. Joshi, R. B. Pachori, A. Vijesh, Classification of ictal and seizure-free eeg signals using fractional linear prediction, Biomedical Signal Processing and Control 9 (2014) 1–5.
- [39] T. I. Rohan, M. S. U. Yusuf, M. Islam, S. Roy, Efficient approach to detect epileptic seizure using machine learning models for modern healthcare system, in: 2020 IEEE Region 10 Symposium (TENSYMP), IEEE, 2020, pp. 1783–1786.
- [40] A. M. Hilal, A. A. Albraikan, S. Dhahbi, M. K. Nour, A. Mohamed, A. Motwakel, A. S. Zamani, M. Rizwanullah, Intelligent epileptic seizure detection and classification model using optimal deep canonical sparse autoencoder, Biology 11 (8) (2022) 1220.

[41] A. M. Hilal, A. A. Albraikan, S. Dhahbi, M. K. Nour, A. Mohamed, A. Mot-wakel, A. S. Zamani, M. Rizwanullah, Intelligent epileptic seizure detection and classification model using optimal deep canonical sparse autoencoder, Biology 11 (8) (2022) 1220.

745

- [42] K. M. Almustafa, Classification of epileptic seizure dataset using different machine learning algorithms, Informatics in Medicine Unlocked 21 (2020) 100444.
- [43] A. H. Osman, A. A. Alzahrani, New approach for automated epileptic disease diagnosis using an integrated self-organization map and radial basis function neural network algorithm, IEEE Access 7 (2018) 4741–4747.
- [44] R. S. Shankar, C. Raminaidu, V. S. Raju, J. Rajanikanth, Detection of epilepsy based on eeg signals using pca with ann model, in: Journal of Physics: Conference Series, Vol. 2070, IOP Publishing, 2021, p. 012145.